9 Quantum Phases and Phase Transitions of Mott Insulators

Subir Sachdev

Department of Physics, Yale University, P.O. Box 208120,
New Haven CT 06520-8120, USA, subir.sachdev@yale.edu

Abstract. This article contains a theoretical overview of the physical properties of antiferromagnetic Mott insulators in spatial dimensions greater than one. Many such materials have been experimentally studied in the past decade and a half, and we make contact with these studies. Mott insulators in the simplest class have an even number of $S = 1/2$ spins per unit cell, and these can be described with quantitative accuracy by the bond operator method: we discuss their spin gap and magnetically ordered states, and the transitions between them driven by pressure or an applied magnetic field. The case of an odd number of $S = 1/2$ spins per unit cell is more subtle: here the spin gap state can spontaneously develop bond order (so the ground state again has an even number of $S = 1/2$ spins per unit cell), and/or acquire topological order and fractionalized excitations. We describe the conditions under which such spin gap states can form, and survey recent theories of the quantum phase transitions among these states and magnetically ordered states. We describe the breakdown of the Landau-Ginzburg-Wilson paradigm at these quantum critical points, accompanied by the appearance of emergent gauge excitations.

9.1 Introduction

The physics of Mott insulators in two and higher dimensions has enjoyed much attention since the discovery of cuprate superconductors. While a quantitative synthesis of theory and experiment in the superconducting materials remains elusive, much progress has been made in describing a number of antiferromagnetic Mott insulators. A number of such insulators have been studied extensively in the past decade, with a few prominent examples being CaV_4O_9 [1], $(C_5H_{12}N_2)_2Cu_2Cl_4$ [2–4], $SrCu_2(BO_3)_2$ [5, 6], $TlCuCl_3$ [7–10], and Cs_2CuCl_4 [11, 12]. In some cases, it has even been possible to tune these insulators across quantum phase transitions by applied pressure [8] or by an applied magnetic field [3,4,7,9]. A useful survey of some of these experiments may be found in the recent article by Matsumoto *et al.* [10].

It would clearly be valuable to understand the structure of the global phase diagram of antiferromagnetic Mott insulators above one dimension. The compounds mentioned above would then correspond to distinct points in this phase diagram, and placing them in this manner should help us better understand the relationship between different materials. One could also

S. Sachdev, Quantum Phases and Phase Transitions of Mott Insulators, Lect. Notes Phys. **645**, 381–432 (2004)
http://www.springerlink.com/

classify the quantum critical points accessed by the pressure or field-tuning experiments. The purpose of this article is to review recent theoretical work towards achieving this goal. We will focus mainly on the case of two spatial dimensions (d), but our methods and results often have simple generalizations to $d = 3$.

One useful vantage point for opening this discussion is the family of Mott insulators with a gap to all spin excitations. All spin gap compounds discovered to date have the important property of being "dimerized", or more precisely, they have an even number of $S = 1/2$ spins per unit cell [13]. In such cases, the spin gap can be understood by adiabatic continuation from the simple limiting case in which the spins form local spin singlets within each unit cell. A simple approach that can be used for a theoretical description of such insulators is the method of bond operators [14,15]. This method has been widely applied, and in some cases provides an accurate quantitative description of numerical studies and experiments [10,16]. We will describe it here in Sect. 9.2 in the very simple context of a coupled dimer antiferromagnet; similar results are obtained in more complicated, and realistic, lattice structures. Sect. 9.2 will also describe the quantum phase transition(s) accessed by varying coupling constants in the Hamiltonian while maintaining spin rotation invariance (this corresponds to experiments in applied pressure): the spin gap closes at a quantum critical point beyond which there is magnetic order. Section 9.2.3 will discuss some of the important experimental consequences of this quantum criticality at finite temperatures. A distinct quantum critical point, belonging to a different universality class, is obtained when the spin gap is closed by an applied magnetic field—this is described in Sect. 9.3.

The remaining sections discuss the theoretically much more interesting and subtle cases of materials with an odd number of $S = 1/2$ spins per unit cell, such as La_2CuO_4 and Cs_2CuCl_4. A complementary, but compatible, perspective on the physics of such antiferromagnets may be found in the review article by Misguich and Lhuillier [17]. Antiferromagnets in this class can develop a spin gap by *spontaneously* breaking the lattice symmetry so that the lattice is effectively dimerized (see discussion in the following paragraph). There are no known materials with a spin gap in which the lattice symmetry has not been broken, but there is a theoretical consensus that spin gap states without lattice symmetry breaking are indeed possible in $d > 1$ [18]. The study of antiferromagnets with an odd number of $S = 1/2$ spins per unit cell is also important for the physics of the doped cuprates. These materials exhibit spin-gap-like behavior at low dopings, and many theories associate aspects of its physics with the spin gap state proximate to the magnetically ordered state of the square lattice antiferromagnet found in La_2CuO_4.

Section 9.4 will describe the nature of a spin gap state on the square lattice. We begin with the nearest-neighbor $S = 1/2$ Heisenberg Hamiltonian on the square lattice—this is known to have a magnetic Néel order which breaks spin rotation invariance. Now add further neighbor exchange couplings until

magnetic order is lost and a spin gap appears. We will show that the ground state undergoes a novel, second-order quantum phase transition to a state with *bond order*: translational symmetry is spontaneously broken [19, 20] so that the resulting lattice structure has an even number of $S = 1/2$ spins per unit cell. So aspects of the non-zero spin excitations in this paramagnet are very similar to the "dimerized" systems considered in Sect. 9.2, and experimentally they will appear to be almost identical. Indeed, it may well be that the experimental materials initially placed in the class of Sect. 9.2, are secretely systems in the class of Sect. 9.4 which have developed bond order driven by the physics of antiferromagets (as in Sect. 9.4.1) at some intermediate energy scale. The host lattice then distorts sympathetically to the bond order, and is effectively dimerized. Such materials will possess many more low-lying singlet excitations than those in the theory of Sect. 9.2: these excitations play an important role in the restoration of translational symmetry as we move towards the Néel state. Unfortunately, such singlet excitations are rather difficult to detect experimentally.

Section 9.5 will address the same issue as Sect. 9.4, but for the case of the triangular lattice. Here the spins are ordered in a non-collinear configuration in the magnetically ordered state, as is observed at low temperatures in Cs_2CuCl_4 [11, 12]. We will argue that in this case there is a route to destruction of magnetic order in which the resulting spin gap state preserves full lattice symmetry [21, 22]. Such a spin gap state has a novel 'topological' order [23] which endows its excitations with charges under an emergent gauge force. Recent experimental measurements of the dynamic structure factor of Cs_2CuCl_4 appear to be described rather well by the excitations of this topologically ordered state at energies above which the magnetic order of the ground state emerges [12, 24].

9.2 Coupled Dimer Antiferromagnet

We begin by describing the quantum phase transition in a simple two-dimensional model of antiferromagnetically coupled $S = 1/2$ Heisenberg spins which has 2 spins per unit cell. The transition is tuned by varying a dimensionless parameter λ. As we noted in Sect. 9.1 different 'dimerized' Mott insulators will correspond to different values of λ, and the value of λ can be tuned by applying pressure [8, 10].

We consider the "coupled dimer" Hamiltonian [25]

$$H_d = J \sum_{\langle ij \rangle \in \mathcal{A}} \mathbf{S}_i \cdot \mathbf{S}_j + \lambda J \sum_{\langle ij \rangle \in \mathcal{B}} \mathbf{S}_i \cdot \mathbf{S}_j, \tag{9.1}$$

where $\mathbf{S}_j$ are spin-1/2 operators on the sites of the coupled-ladder lattice shown in Fig. 9.1, with the $\mathcal{A}$ links forming decoupled dimers while the $\mathcal{B}$ links couple the dimers as shown. The ground state of H_d depends only on

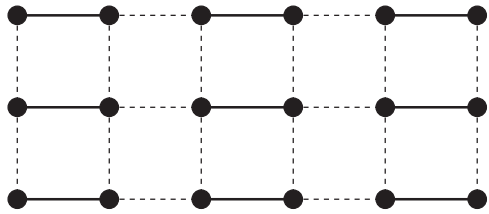

Fig. 9.1. The coupled dimer antiferromagnet. Spins ($S = 1/2$) are placed on the sites, the $\mathcal{A}$ links are shown as full lines, and the $\mathcal{B}$ links as dashed lines.

the dimensionless coupling λ, and we will describe the low temperature (T) properties as a function of λ. We will restrict our attention to $J > 0$ and $0 \leq \lambda \leq 1$.

Note that exactly at $\lambda = 1$, H_d is identical to the square lattice antiferromagnet, and this is the only point at which the Hamiltonian has only one spin per unit cell. At all other values of λ H_d has a pair of $S = 1/2$ spins in each unit cell of the lattice. As will become clear from our discussion, this is a key characteristic which permits a simple theory for the quantum phase transition exhibited by H_d. Models with only a single $S = 1/2$ spin per unit cell usually display far more complicated behavior, and will be discussed in Sects. 9.4,9.5.

We will begin with a physical discussion of the phases and excitations of the coupled dimer antiferromagnet, H_d in Sect. 9.2.1. We will propose a quantum field-theoretical description of this model in Sect. 9.2.2: we will verify that the limiting regimes of the field theory contain excitations whose quantum numbers are in accord with the phases discussed in Sect. 9.2.1, and will then use the field theory to describe the quantum critical behavior both at zero and finite temperatures.

9.2.1 Phases and Their Excitations

Let us first consider the case where λ is close to 1. Exactly at $\lambda = 1$, H_d is identical to the square lattice Heisenberg antiferromagnet, and this is known to have long-range, magnetic Néel phase in its ground state *i.e.* the spin-rotation symmetry is broken and the spins have a non-zero, staggered, expectation value in the ground state with

$$\langle \mathbf{S}_j \rangle = \eta_j N_0 \mathbf{n}, \tag{9.2}$$

where $\mathbf{n}$ is some fixed unit vector in spin space, η_j is ± 1 on the two sublattices, and N_0 is the Néel order parameter. This long-range order is expected to be preserved for a finite range of λ close to 1. The low-lying excitations above the ground state consist of slow spatial deformations in the orientation $\mathbf{n}$: these are the familiar spin waves, and they can carry arbitrarily low energy *i.e.* the phase is 'gapless'. The spectrum of the spin waves can be

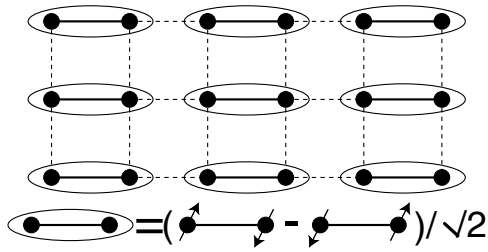

Fig. 9.2. Schematic of the quantum paramagnet ground state for small λ. The ovals represent singlet valence bond pairs.

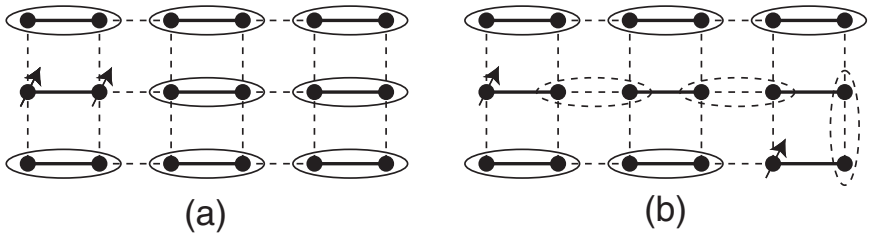

Fig. 9.3. (a) Cartoon picture of the bosonic $S = 1$ excitation of the paramagnet. (b) Fission of the $S = 1$ excitation into two $S = 1/2$ spinons. The spinons are connected by a "string" of valence bonds (denoted by dashed ovals) which lie on weaker bonds; this string costs a finite energy per unit length and leads to the confinement of spinons.

obtained from a text-book analysis of small fluctuations about the ordered Néel state using the Holstein-Primakoff method [26]: such an analysis yields *two* polarizations of spin waves at each wavevector $k = (k_x, k_y)$ (measured from the antiferromagnetic ordering wavevector), and they have excitation energy $\varepsilon_k = (c_x^2 k_x^2 + c_y^2 k_y^2)^{1/2}$, with c_x, c_y the spin-wave velocities in the two spatial directions.

Let us turn now to the vicinity of $\lambda = 0$. Exactly at $\lambda = 0$, H_d is the Hamiltonian of a set of decoupled dimers, with the simple exact ground state wavefunction shown in Fig. 9.2: the spins in each dimer pair into valence bond singlets, leading to a paramagnetic state which preserves spin rotation invariance and all lattice symmetries. Excitations are now formed by breaking a valence bond, which leads to a *three*-fold degenerate state with total spin $S = 1$, as shown in Fig. 9.3a. At $\lambda = 0$, this broken bond is localized, but at finite λ it can hop from site-to-site, leading to a triplet quasiparticle excitation. Note that this quasiparticle is *not* a spin-wave (or equivalently, a 'magnon') but is more properly referred to as a spin 1 *exciton* or a *triplon* [27]. We parameterize its energy at small wavevectors k (measured from the minimum of the spectrum in the Brillouin zone) by

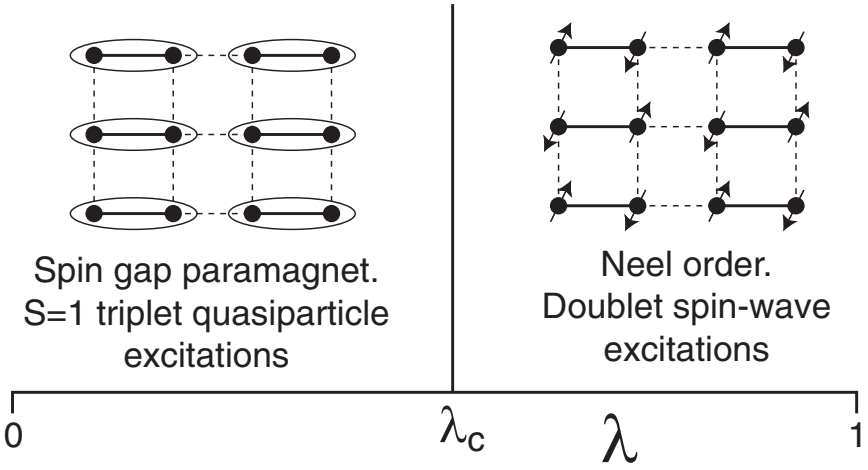

Fig. 9.4. Ground states of H_d as a function of λ The quantum critical point is at [28] $\lambda_c = 0.52337(3)$. The compound $TlCuCl_3$ undergoes a similar quantum phase transition under applied pressure [8].

$$\varepsilon_k = \Delta + \frac{c_x^2 k_x^2 + c_y^2 k_y^2}{2\Delta}, \tag{9.3}$$

where Δ is the spin gap, and c_x, c_y are velocities; we will provide an explicit derivation of (9.3) in Sect. 9.2.2. Figure 9.3 also presents a simple argument which shows that the $S = 1$ exciton cannot fission into two $S = 1/2$ 'spinons'.

The very distinct symmetry signatures of the ground states and excitations between $\lambda \approx 1$ and $\lambda \approx 0$ make it clear that the two limits cannot be continuously connected. It is known that there is an intermediate second-order phase transition at [25, 28] $\lambda = \lambda_c = 0.52337(3)$ between these states as shown in Fig. 9.4. Both the spin gap Δ and the Néel order parameter N_0 vanish continuously as λ_c is approached from either side.

9.2.2 Bond Operators and Quantum Field Theory

In this section we will develop a continuum description of the low energy excitations in the vicinity of the critical point postulated above. There are a number of ways to obtain the same final theory: here we will use the method of *bond operators* [14, 15], which has the advantage of making the connection to the lattice degrees of freedom most direct. We rewrite the Hamiltonian using bosonic operators which reside on the centers of the $\mathcal{A}$ links so that it is explicitly diagonal at $\lambda = 0$. There are 4 states on each $\mathcal{A}$ link ($|\uparrow\uparrow\rangle$, $|\uparrow\downarrow\rangle$, $|\downarrow\uparrow\rangle$, and $|\downarrow\downarrow\rangle$) and we associate these with the canonical singlet boson s and the canonical triplet bosons t_α ($\alpha = x, y, z$) so that

$$|s\rangle \equiv s^\dagger|0\rangle = \frac{1}{\sqrt{2}}\left(|\uparrow\downarrow\rangle - |\downarrow\uparrow\rangle\right) \quad ; \quad |t_x\rangle \equiv t_x^\dagger|0\rangle = \frac{-1}{\sqrt{2}}\left(|\uparrow\uparrow\rangle - |\downarrow\downarrow\rangle\right) \quad ;$$
$$|t_y\rangle \equiv t_y^\dagger|0\rangle = \frac{i}{\sqrt{2}}\left(|\uparrow\uparrow\rangle + |\downarrow\downarrow\rangle\right) \quad ; \quad |t_z\rangle \equiv t_z^\dagger|0\rangle = \frac{1}{\sqrt{2}}\left(|\uparrow\downarrow\rangle + |\downarrow\uparrow\rangle\right). \quad (9.4)$$

Here $|0\rangle$ is some reference vacuum state which does not correspond to a physical state of the spin system. The physical states always have a single bond boson and so satisfy the constraint

$$s^\dagger s + t_\alpha^\dagger t_\alpha = 1. \quad (9.5)$$

By considering the various matrix elements $\langle s|\mathbf{S}_1|t_\alpha\rangle$, $\langle s|\mathbf{S}_2|t_\alpha\rangle$, ..., of the spin operators $\mathbf{S}_{1,2}$ on the ends of the link, it follows that the action of $\mathbf{S}_1$ and $\mathbf{S}_2$ on the singlet and triplet states is equivalent to the operator identities

$$S_{1\alpha} = \frac{1}{2}\left(s^\dagger t_\alpha + t_\alpha^\dagger s - i\epsilon_{\alpha\beta\gamma} t_\beta^\dagger t_\gamma\right),$$
$$S_{2\alpha} = \frac{1}{2}\left(-s^\dagger t_\alpha - t_\alpha^\dagger s - i\epsilon_{\alpha\beta\gamma} t_\beta^\dagger t_\gamma\right), \quad (9.6)$$

where α,β,γ take the values x,y,z, repeated indices are summed over and ϵ is the totally antisymmetric tensor. Inserting (9.6) into (9.1), and using (9.5), we find the following Hamiltonian for the bond bosons:

$$H_d = H_0 + H_1$$
$$H_0 = J\sum_{\ell\in\mathcal{A}}\left(-\frac{3}{4}s_\ell^\dagger s_\ell + \frac{1}{4}t_{\ell\alpha}^\dagger t_{\ell\alpha}\right)$$
$$H_1 = \lambda J\sum_{\ell,m\in\mathcal{A}}\Bigg[a(\ell,m)\left(t_{\ell\alpha}^\dagger t_{m\alpha} s_m^\dagger s_\ell + t_{\ell\alpha}^\dagger t_{m\alpha}^\dagger s_m s_\ell + \text{H.c.}\right) + b(\ell,m)$$
$$\times\left(i\epsilon_{\alpha\beta\gamma} t_{m\alpha}^\dagger t_{\ell\beta}^\dagger t_{\ell\gamma} s_m + \text{H.c.}\right) + c(\ell,m)\left(t_{\ell\alpha}^\dagger t_{m\alpha}^\dagger t_{m\beta} t_{\ell\beta} - t_{\ell\alpha}^\dagger t_{m\beta}^\dagger t_{m\alpha} t_{\ell\beta}\right)\Bigg] \quad (9.7)$$

where ℓ, m label links in $\mathcal{A}$, and a, b, c are numbers associated with the lattice couplings which we will not write out explicitly. Note that $H_1 = 0$ at $\lambda = 0$, and so the spectrum of the paramagnetic state is fully and exactly determined. The main advantage of the present approach is that application of the standard methods of many body theory to (9.7), while imposing the constraint (9.5), gives a very satisfactory description of the phases with $\lambda \neq 0$, including across the transition to the Néel state. In particular, an important feature of the bond operator approach is that the simplest mean field theory already yields ground states and excitations with the correct quantum numbers; so a strong fluctuation analysis is not needed to capture the proper physics.

A complete numerical analysis of the properties of (9.7) in a self-consistent Hartree-Fock treatment of the four boson terms in H_1 has been presented

in [14]. In all phases the s boson is well condensed at zero momentum, and the important physics can be easily understood by examining the structure of the low energy action for the t_α bosons. For the particular Hamiltonian (9.1), the spectrum of the t_α bosons has a minimum at the momentum $(0, \pi)$, and for large enough λ the t_α condense at this wavevector: the representation (9.6) shows that this condensed state is the expected Néel state, with the magnetic moment oscillating as in (9.2). The condensation transition of the t_α is therefore the quantum phase transition between the paramagnetic and Néel phases of the coupled dimer antiferromagnet. In the vicinity of this critical point, we can expand the t_α bose field in gradients away from the $(0, \pi)$ wavevector: so we parameterize

$$t_{\ell,\alpha}(\tau) = t_\alpha(r_\ell, \tau) e^{i(0,\pi)\cdot \boldsymbol{r}_\ell} \tag{9.8}$$

where τ is imaginary time, $r \equiv (x, y)$ is a continuum spatial coordinate, and expand the effective action in spatial gradients. In this manner we obtain

$$\mathcal{S}_t = \int d^2 r d\tau \left[t_\alpha^\dagger \frac{\partial t_\alpha}{\partial \tau} + C t_\alpha^\dagger t_\alpha - \frac{D}{2} \left(t_\alpha t_\alpha + \text{H.c.} \right) + K_{1x} |\partial_x t_\alpha|^2 + K_{1y} |\partial_y t_\alpha|^2 \right.$$
$$\left. + \frac{1}{2} \left(K_{2x} (\partial_x t_\alpha)^2 + K_{2y} (\partial_y t_\alpha)^2 + \text{H.c.} \right) + \cdots \right]. \tag{9.9}$$

Here $C, D, K_{1,2x,y}$ are constants that are determined by the solution of the self-consistent equations, and the ellipses represent terms quartic in the t_α. The action $\mathcal{S}_t$ can be easily diagonalized, and we obtain a $S = 1$ quasiparticle excitation with the spectrum

$$\varepsilon_k = \left[\left(C + K_{1x} k_x^2 + K_{1y} k_y^2 \right)^2 - \left(D + K_{2x} k_x^2 + K_{2y} k_y^2 \right)^2 \right]^{1/2}. \tag{9.10}$$

This is, of course, the triplon (or spin exciton) excitation of the paramagnetic phase postulated earlier in (9.3); the latter result is obtained by expanding (9.10) in momenta, with $\Delta = \sqrt{C^2 - D^2}$. This value of Δ shows that the ground state is paramagnetic as long as $C > D$, and the quantum critical point to the Néel state is at $C = D$.

The critical point and the Néel state are more conveniently described by an alternative formulation of $\mathcal{S}_t$ (although an analysis using bond operators directly is also possible [29]). It is useful to decompose the complex field t_α into its real and imaginary parts as follows

$$t_\alpha = Z(\varphi_\alpha + i\pi_\alpha), \tag{9.11}$$

where Z is a normalization chosen below. Insertion of (9.11) into (9.9) shows that the field π_α has a quadratic term $\sim (C + D)\pi_\alpha^2$, and so the coefficient of π_α^2 remains large even as the spin gap Δ becomes small. Consequently, we can safely integrate π_α out, and the resulting action for φ_α takes the form

$$\mathcal{S}_\varphi = \int d^2r d\tau \left[\frac{1}{2} \left\{ (\partial_\tau \varphi_\alpha)^2 + c_x^2 (\partial_x \varphi_\alpha)^2 + c_y^2 (\partial_y \varphi_\alpha)^2 + s\varphi_\alpha^2 \right\} + \frac{u}{24} \left(\varphi_\alpha^2 \right)^2 \right]. \tag{9.12}$$

Here we have chosen Z to fix the coefficient of the temporal gradient term, and $s = C^2 - D^2$.

The formulation $\mathcal{S}_\varphi$ makes it simple to explore the physics in the region $s < 0$. It is clear that the effective potential of φ_α has a minimum at a non-zero φ_α, and that $\langle \varphi_\alpha \rangle \propto N_0$, the Néel order parameter in (9.2). It is simple to carry out a small fluctuation analysis about this saddle point, and we obtain the doublet of gapless spin-wave modes advertised earlier.

We close this subsection by noting that all of the above results have a direct generalization to other lattices, and also to spin systems in three dimensions. Matsumoto *et al.* [10] have applied the bond operator method to $TlCuCl_3$ and obtained good agreement with experimental observations. One important difference that emerges in such calculations on some frustrated lattices [30] is worth noting explicitly here: the minimum of the t_α spectrum need not be at special wavevector like $(0, \pi)$, but can be at a more generic wavevector $\boldsymbol{Q}$ such that $\boldsymbol{Q}$ and $-\boldsymbol{Q}$ are not separated by a reciprocal lattice vector. A simple example which we consider here is an extension of (9.1) in which there are additional exchange interactions along all diagonal bonds oriented 'north-east' (so that the lattice has the connectivity of a triangular lattice). In such cases, the structure of the low energy action is different, as is the nature of the magnetically ordered state. The parameterization (9.8) must be replaced by

$$t_{\ell\alpha}(\tau) = t_{1\alpha}(r_\ell, \tau) e^{i\boldsymbol{Q}\cdot\boldsymbol{r}_\ell} + t_{2\alpha}(r_\ell, \tau) e^{-i\boldsymbol{Q}\cdot\boldsymbol{r}_\ell}, \tag{9.13}$$

where $t_{1,2\alpha}$ are independent complex fields. Proceeding as above, we find that the low energy effective action (9.12) is replaced by

$$\mathcal{S}_\Phi = \int d^2r d\tau \Bigg[|\partial_\tau \Phi_\alpha|^2 + c_x^2 |\partial_x \Phi_\alpha|^2 + c_y^2 |\partial_y \Phi_\alpha|^2 + s |\Phi_\alpha|^2 + \frac{u}{2} \left(|\Phi_\alpha|^2 \right)^2 + \frac{v}{2} |\Phi_\alpha^2|^2 \Bigg], \tag{9.14}$$

where now Φ_α is a *complex* field such that $\langle \Phi_\alpha \rangle \sim \langle t_{1\alpha} \rangle \sim \langle t_{2\alpha}^\dagger \rangle$. Notice that there is now a second quartic term with coefficient v. If $v > 0$, configurations with $\Phi_\alpha^2 = 0$ are preferred: in such configurations $\Phi_\alpha = n_{1\alpha} + i n_{2\alpha}$, where $n_{1,2\alpha}$ are two equal-length orthogonal vectors. Then from (9.13) and (9.6) it is easy to see that the physical spins possess *spiral* order in the magnetically ordered state in which Φ_α is condensed. A spiral state is illustrated in Fig. 9.13, and we will have more to say about this state in Sect. 9.5. For the case $v < 0$, the optimum configuration has $\Phi_\alpha = n_\alpha e^{i\theta}$ where n_α is a real vector: this leads to a magnetically ordered state with spins polarized *collinearly* in a spin density wave at the wavevector $\boldsymbol{Q}$.

9.2.3 Quantum Criticality

We will restrict our discussion here to the critical point described by $\mathcal{S}_\varphi$. Similar results apply to $\mathcal{S}_\Phi$ for the parameter regime in which it exhibits a second order transition [31]. Experimentally, the results below are relevant to materials that can be tuned across the magnetic ordering transition by applied pressure (such as $TlCuCl_3$ [8]), or to materials which happen to be near a critical point at ambient pressure (such as $LaCuO_{2.5}$ [32]).

The field theory $\mathcal{S}_\varphi$ is actually a familiar and well-studied model in the context of classical critical phenomena. Upon interpreting τ as a third spatial coordinate, $\mathcal{S}_\varphi$ becomes the theory of a classical O(3)-invariant Heisenberg ferromagnet at finite temperatures (in general a d dimensional quantum antiferromagnet will map to a $d+1$ dimensional classical Heisenberg ferromagnet at finite temperature [33]). The Curie transition of the Heisenberg ferromagnet then maps onto the quantum critical point between the paramagnetic and Néel states described above. A number of important implications for the quantum problem can now be drawn immediately.

The theory $\mathcal{S}_\varphi$ has a 'relativistic' invariance, and consequently the dynamic critical exponent must be $z = 1$. The spin correlation length will diverge at the quantum critical point with the exponent [34] $\nu = 0.7048(30)$. The spin gap of the paramagnet, Δ, vanishes as $\Delta \sim (\lambda_c - \lambda)^{z\nu}$, and this prediction is in excellent agreement with the numerical study of the dimerized antiferromagnet [28].

A somewhat more non-trivial consequence of this mapping is in the structure of the spectrum at the critical point $\lambda = \lambda_c$. At the Curie transition of the classical ferromagnet it is known [35] that spin correlations decay as $\sim 1/p^{2-\eta}$, where p is the 3-component momentum in the 3-dimensional classical space. We can now analytically continue this expression from its p_z dependence in the third classical dimension to the real frequency, ω, describing the quantum antiferromagnet. This yields the following fundamental result for the dynamic spin susceptibility, $\chi(k, \omega)$, at the $T = 0$ quantum critical point of the coupled-dimer antiferromagnet:

$$\chi(k, \omega) \sim \frac{1}{\left(c_x^2 k_x^2 + c_y^2 k_y^2 - (\omega + i\epsilon)^2\right)^{1-\eta/2}}, \tag{9.15}$$

where ϵ is a positive infinitesimal. Note that in (9.15) the momentum k is measured from the (π, π) ordering wavevector of the Néel state. The exponent η is the same as that of the classical Heisenberg ferromagnet, and has a rather small value [34]: $\eta \approx 0.03$. However, the non-zero η does make a significant difference to the physical interpretation of the excitations at the critical point. In particular note that $\mathrm{Im}\chi(k, \omega)$ does not have a pole at any k, but rather a continuum spectral weight above a threshold energy [36, 37]

$$\mathrm{Im}\chi(k,\omega) \sim \mathrm{sgn}(\omega)\sin\left(\frac{\pi\eta}{2}\right)\frac{\theta\left(|\omega| - \sqrt{c_x^2k_x^2 + c_y^2k_y^2}\right)}{\left(\omega^2 - c_x^2k_x^2 - c_y^2k_y^2\right)^{1-\eta/2}}, \tag{9.16}$$

where θ is the unit step function. This indicates there are no quasiparticles at the critical point, and only a dissipative critical continuum.

There is also some very interesting structure in the quantum critical dynamic response at nonzero T [36,37]. Here, one way to understand the physics is to approach the critical point from the paramagnetic side ($\lambda < \lambda_c$). As we noted earlier, the paramagnetic phase has well-defined 'triplon' or 'spin exciton' excitations t_α, and these have an infinite lifetime at $T = 0$. At $T > 0$, thermally excited t_α quasiparticles will collide with each other via their scattering amplitude, u, and this will lead to a finite lifetime [37,38]. Now approach $\lambda = \lambda_c$. The renormalization group analysis of $\mathcal{S}_\varphi$ tells us that the quartic coupling u approaches a fixed point value in the critical region. This means that u is no longer an arbitrary parameter, and an appropriately defined t_α scattering amplitude must also acquire universal behavior. In particular, the t_α lifetime is determined by the only energy scale available, which is k_BT. So we have the remarkable result that the characteristic spin relaxation time is a universal number times $\hbar/(k_BT)$. More precisely, we can write for the local dynamic spin susceptibility $\chi_L(\omega) = \int d^2k\chi(k,\omega)$ the universal scaling form

$$\mathrm{Im}\chi_L(\omega) = T^\eta F\left(\frac{\hbar\omega}{k_BT}\right). \tag{9.17}$$

Here F is a universal function which has the limiting behaviors

$$F(\overline{\omega}) \sim \begin{cases} \overline{\omega} & , |\overline{\omega}| \ll 1 \\ \mathrm{sgn}(\omega)|\overline{\omega}|^\eta & , |\overline{\omega}| \gg 1 \end{cases}. \tag{9.18}$$

Note that F has a smooth linear behavior in the regime $|\hbar\omega| \ll k_BT$, and this is similar to any simple dissipative system. The difference here is that the coefficient of dissipation is determined by k_BT alone.

The quantum critical behavior described here is expected to apply more generally to other correlated electron systems, provided the critical theory has non-linear couplings which approach fixed point values.

9.3 Influence of an Applied Magnetic Field

An important perturbation that can be easily applied to antiferromagnets in the class discussed in Sect. 9.2 is a uniform magnetic field. The Zeeman energy in available fields can often be comparable to the typical antiferromagnetic exchange constant J, and so the ground state can be perturbed significantly. It is therefore of interest to understand the evolution of the phase diagram in Fig. 9.4 under an applied field of arbitrary strength.

We are interested here in the evolution of the ground state as a function of B where the Hamiltonian H_d in (9.1) is transformed as

$$H_d \to H_d - \sum_j \mathbf{B} \cdot \mathbf{S}_j. \tag{9.19}$$

Most of the basic features can actually be understood quite easily in a simple extension of the self-consistent Hartree-Fock theory of bond bosons that was discussed in Sect. 9.2.2. Under the transformation (9.19), it is easily seen from (9.6) that

$$H_d \to H_d + iB_\alpha \sum_{\ell \in \mathcal{A}} \epsilon_{\alpha\beta\gamma} t^\dagger_{\ell\beta} t_{\ell\gamma}. \tag{9.20}$$

The presence of a non-zero B breaks spin rotation invariance and so all the self-consistent expectation values of operator bilinears have to reflect this reduced symmetry in the Hartree-Fock theory. Apart from this the mechanics of the computation mostly remain the same. However, for stronger fields, it is sometimes necessary to allow for broken translational symmetry in the expectation values, as the ground state can acquire a modulated structure.

We will discuss the results of such an analysis in weak and strong fields in the following subsections.

9.3.1 Weak Fields

For weak fields applied to the paramagnet (specifically, for fields $B < \Delta$, the influence of (9.20) can be understood exactly. The coupling to B involves an operator which commutes with the remaining Hamiltonian (the total spin), and hence the wavefunction of the ground state remains insensitive to the value of B. The same applies to the wavefunctions of the excited states. However, the excited states can have non-zero total spin and so their energies do depend upon B. In particular the triplet t_α quasiparticle with energy (9.3) or (9.10) carries total spin $S = 1$, and consequently we conclude that this triplet splits according to

$$\varepsilon_k \to \varepsilon_k - mB \tag{9.21}$$

with $m = 0, \pm 1$. Note that the lowest energy quasiparticle (with $m = 1$) has a positive energy as long as $B < \Delta$, and this is required for the stability of the paramagnet. So the phase boundary of the paramagnetic phase is exactly $B = \Delta$, and using $\Delta \sim (\lambda_c - \lambda)^{z\nu}$, we can sketch the boundary of the paramagnetic phase as in Fig. 9.5.

What happens beyond the paramagnetic phase? As in Sect. 9.2.2, we answer this question by using the transformation (9.11), and by examining the analog of $\mathcal{S}_\varphi$ under a non-zero B. Using (9.20), and integrating out π_α, we now find that the action $\mathcal{S}_\varphi$ in (9.12) remains unchanged apart from the mapping [40]

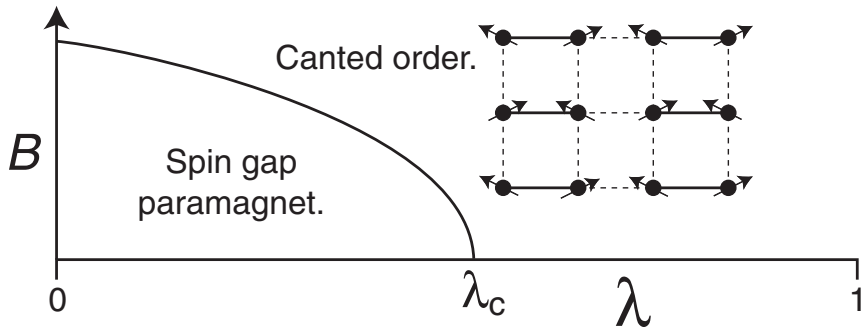

Fig. 9.5. Evolution of the phases of Fig. 9.4 under a weak field B (magnetization plateau at large B, appearing in Fig. 9.6, are not shown). The paramagnetic phase has exactly the same ground state wavefunction as that at $B = 0$. The phase boundary behaves like $B \sim (\lambda_c - \lambda)^{z\nu}$. The B field is oriented vertically upwards, and the static moments in the canted phase can rotate uniformly about the vertical axis. The phase boundary at non-zero B is described by the $z = 2$ dilute Bose gas quantum critical theory. The phase diagram of $TlCuCl_3$ in applied pressure and magnetic field looks similar to the one above [10]. The corresponding phase diagram of the field-induced magnetic ordering transition of a superconductor (rather than a Mott insulator) has been investigated recently [39], and successfully applied to experiments on the doped cuprates; this phase diagram of the superconductor has significant differences from the one above.

$$(\partial_\tau \varphi_\alpha)^2 \to (\partial_\tau \varphi_\alpha + i\epsilon_{\alpha\beta\gamma} B_\beta \varphi_\gamma)^2 . \tag{9.22}$$

The action (9.12), (9.22) can now be analyzed by a traditional small fluctuation analysis about $\varphi_\alpha = 0$. Let us assume that $\mathbf{B} = (0, 0, B)$ is oriented along the z axis. Then the coefficient of φ_z^2 is s, while that of $\varphi_x^2 + \varphi_y^2$ is $s - B^2$. This suggests that we focus only on the components of φ_α in the plane orthogonal to $\mathbf{B}$, and integrate out the component of φ_α along the direction of $\mathbf{B}$. Indeed, if we define

$$\Psi = \frac{\varphi_x + i\varphi_y}{\sqrt{B}} \tag{9.23}$$

and integrate out φ_z, then we obtain from (9.12), (9.22) the effective action for Ψ:

$$\mathcal{S}_\Psi = \int d^2 r d\tau \left[\Psi^* \partial_\tau \Psi + \frac{c_x^2}{2B} |\partial_x \Psi|^2 + \frac{c_y^2}{2B} |\partial_y \Psi|^2 - \mu |\Psi|^2 + \frac{u}{24B} |\Psi|^4 \right] . \tag{9.24}$$

Here, $\mu = (s - B^2)/2B$, and we have retained only leading order temporal and spatial gradients and the leading dependence of u. Clearly, this is the theory of a Bose gas in the grand canonical ensemble at a chemical potential

μ, with a repulsive short-range interaction [41]. At $T = 0$, and $\mu < 0$, such a theory has a ground state which is simply the vacuum with no Bose particles. Here, this vacuum state corresponds to the spin gap antiferromagnet, and the B-independence of the ground state of the antiferromagnet corresponds here to the μ independence of the ground state of $\mathcal{S}_\Psi$. There is an onset of a finite density of bosons in $\mathcal{S}_\Psi$ for $\mu > 0$, and this onset therefore corresponds to the quantum phase transition in the antiferromagnet at $B = \Delta$. So we must have $\mu = 0$ in $\mathcal{S}_\Psi$ at precisely the point where $B = \Delta$: the value of μ quoted above shows that this is true at zeroth order in u, and higher order terms in u must conspire to maintain this result.

The above analysis makes it clear that the $\mu \geq 0$ region of $\mathcal{S}_\Psi$ will describe the quantum phase transition out of the paramagnet at non-zero B. This transition is merely the formation of a Bose-Einstein condensate of the $m = 1$ component of the triplon bosons. For $\mu > 0$ we have a finite density of Ψ bosons which Bose condense in the ground state, so that $\langle \Psi \rangle \neq 0$. From (9.23) we see that this Bose condensation corresponds to antiferromagnetic order in the plane perpendicular to $\mathbf{B}$. Indeed, the phase of this Bose condensate is simply the orientation of the spins in the x, y plane, and so here this phase is directly observable. Further, by taking derivatives of (9.19) and $\mathcal{S}_\Psi$ w.r.t. B, we see that the density of bosons is proportional to the magnetization per spin, Ω, in the direction parallel to $\mathbf{B}$:

$$\Omega \equiv \frac{1}{N} \sum_j \langle S_{jz} \rangle \propto \langle |\Psi|^2 \rangle, \tag{9.25}$$

where N is the total number of spins. Consequently, the average magnetic moments in the non-paramagnetic phase are in a 'canted' configuration, as shown in Fig. 9.5. The quantum phase transition between the paramagnet and the canted state is described by the theory of the density onset in a Bose gas: this theory has $z = 2$, $\nu = 1/2$, and an upper critical dimension of $d = 2$ [41, 42].

We conclude this section by noting that interesting recent work [43] has examined the Bose-Einstein condensation of the $m = 1$ triplon bosons in a *random* potential. This is achieved by studying $Tl_{1-x}K_xCuCl_3$, where the stoichiometric disorder among the non-magnetic ions acts as a random potential on the triplons.

9.3.2 Strong Fields

We have seen above that applying a magnetic field eventually leads to the onset of a ferromagnetic moment in the directions of the applied field. How does this moment evolve as we continue to increase the field? Eventually, B will become so large that it pays to have all the spins polarized in the direction of the field: this corresponds to a saturation in the magnetization, and making B even stronger will not change the ground state. In terms of the

t bosons, this fully polarized state, $|FP\rangle$, with $\Omega = 1/2$, is seen from (9.20) or (9.4) to correspond exactly to

$$|FP\rangle = \prod_{\ell} \frac{(t^{\dagger}_{\ell x} + it^{\dagger}_{\ell y})}{\sqrt{2}} |0\rangle. \tag{9.26}$$

So there must be at least one more quantum phase transition as a B is increased: this is transition from the $|FP\rangle$ state at very large B to a state with a continuously varying ferromagnetic moment which eventually reaches the saturation value from below.

A theory for the transition away from the $|FP\rangle$ state with decreasing B can be developed using methods very similar to those used in Sect. 9.2.2 and 9.3.1. We treat the quartic terms in (9.7) in a Hartree-Fock approximation, and examine small fluctuations away from the $|FP\rangle$ state. These are dominated by excitation which create t_z quanta (which have $m = 0$) on the dimers, and so the effective theory is expressed in terms of

$$\widetilde{\Psi}^{\dagger} \sim t^{\dagger}_{z}(t_x - it_y). \tag{9.27}$$

Indeed, it is not difficult to see that the resulting theory for $\widetilde{\Psi}$ has exactly the same form as (9.24). Now the μ for $\widetilde{\Psi}$ decreases with increasing B, and we have $\mu = 0$ at the critical field at which $|FP\rangle$ first becomes the ground state. Furthermore, $\langle|\widetilde{\Psi}|^2\rangle$ now measures the deviation away from $\Omega = 1/2$. Apart from this 'inversion' in the field axis, it is clear that the universality class of the present transition is identical to that discussed in Sect. 9.3.1.

A further possibility for a plateau in the value of Ω with increasing B is worth mentioning [44], as analogs are realized in $SrCu_2(BO_3)_2$ [45] and NH_4CuCl_3 [46]. So far we have found plateaus at $\Omega = 0$ for $B < \Delta$, and at $\Omega = 1/2$ for large B. For the $\Omega = 1/2$ state we had every dimer with a $(t^{\dagger}_x + it^{\dagger}_y)/\sqrt{2}$ boson. Now imagine that these bosons form a Wigner-crystalline state so that there are p such bosons for every q dimers; here $0 \leq p \leq q$, $q \geq 1$, are integers. Such a state will have $\Omega = p/(2q)$, and breaks the translational symmetry of the underlying dimer antiferromagnet such that there are q dimers per unit cell (or $2q$ spins per unit cell). The energy gap towards boson motion in the Wigner crystal (*i.e.* its incompressibility) will ensure that Ω is stable under small variations of B. In this manner we can obtain a magnetization plateau at $\Omega = p/(2q)$ in a state with a unit cell of q dimers.

We summarize the considerations of this subsection in Fig. 9.6, showing a possible evolution of Ω in a model similar to H_d in (9.1). As we have already noted, the plateau onset transitions at $\Omega = 0$ and $\Omega = 1/2$ are both described by the $z = 2$ dilute Bose gas theory (9.24). The transitions in and out of other fractional plateaus are potentially more complicated because these involve spontaneous breaking of translational symmetry. The translation symmetry could be restored at the same point at which there is onset of superfluid

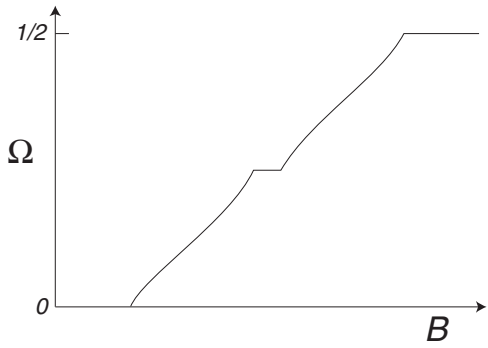

Fig. 9.6. Magnetization density, Ω, defined in (9.25) as a function of the applied magnetic field. The plateau shown at $\Omega = 0$ is present provided the zero field state is a paramagnet *i.e.* $\lambda < \lambda_c$. The full saturation plateau at $\Omega = 1/2$ is always present. The plateau at $\Omega = 1/4$ is not present in the nearest-neighbor model H_d in (9.1), but it is believed that such a plateau will appear upon including frustrating exchange interactions; this plateau will involve a broken translational symmetry in the coupled dimer antiferromagnet. Such magnetization plateaux are found in $SrCu_2(BO_3)_2$ [45] and NH_4CuCl_3 [46]

order—this is possibly a first order transition with a jump in the value of Ω. Alternatively, there could be an intermediate 'supersolid' phase, in which case the plateau transition has the same broken translational symmetry on both sides of it, placing it also in the class of (9.24).

9.4 Square Lattice Antiferromagnet

This section will address the far more delicate problem of quantum phase transitions in antiferromagnets with an odd number of $S = 1/2$ spins per unit cell. We will mainly concern ourselves with square lattice Hamiltonians of the form

$$H_s = J \sum_{\langle ij \rangle} \mathbf{S}_i \cdot \mathbf{S}_j + \ldots . \tag{9.28}$$

Here J is a nearest-neighbor antiferromagnetic exchange and the ellipses represent further short-range exchange interactions (possibly involving multiple spin ring exchange) which preserve the full symmetry of the square lattice. The model H_d is a member of the class H_s only at $\lambda = 1$; at other values of λ the symmetry group of the square lattice is explicitly broken, and the doubling of the unit cell was crucial in the analysis of Sect. 9.2. With full square lattice symmetry, the paramagnetic phase is not determined as simply as in the small λ expansion, and we have to account more carefully for the 'resonance' between different valence bond configurations.

One ground state of H_s is, of course, the Néel state characterized by (9.2); this is obtained in the absence of the interactions denoted by ellipses in (9.28). Now imagine tuning the further neighbor couplings in (9.28) so that spin rotation invariance is eventually restored and we obtain a paramagnetic ground state. We can divide the possibilities for this state into two broad classes, which we discuss in turn.

In the first class of paramagnets, no symmetries of the Hamiltonian are broken, and the spins have paired with each other into valence bond singlets which strongly resonate between the large number of possible pairings: this is a resonating valence bond (RVB) liquid [47,48]. We will discuss such states further in Sect. 9.5: they have a connection with magnetically ordered states with non-collinear magnetic order, unlike the collinear Néel state of the nearest neighbor square lattice antiferromagnet.

In the second class of paramagnets, the valence bond singlets spontaneously crystallize into some configuration which necessarily breaks a lattice symmetry. A simple example of such a *bond-ordered* paramagnet is the columnar state we have already considered in Fig. 9.2. For the dimerized antiferromagnet H_d, the bond configuration in Fig. 9.2 was chosen explicitly in the Hamiltonian by the manner in which we divided the links into classes $\mathcal{A}$ and $\mathcal{B}$ for $\lambda \neq 1$. For H_s, there is no such distinction between the links, and hence a state like Fig. 9.2 *spontaneously* breaks a lattice symmetry. Furthermore, there are 3 other equivalent states, obtained by successive 90 degree rotations of Fig. 9.2 about any lattice site, which are completely equivalent. So for H_s, the bond-ordered paramagnet in Fig. 9.2 is four-fold degenerate. Going beyond simple variational wavefunctions like Fig. 9.2, the bond-ordered states are characterized by a bond order parameter

$$Q_{ij} = \langle \mathbf{S}_i \cdot \mathbf{S}_j \rangle; \tag{9.29}$$

the values of Q_{ij} on the links of the lattice in a bond-ordered state have a lower symmetry than the values of the exchange constants J_{ij} in the Hamiltonian. We will develop an effective model for quantum fluctuations about the collinear Néel state in H_s below, and will find that such bond-ordered paramagnets emerge naturally [19].

Let us now try to set up a theory for quantum fluctuations about the Néel state (9.2). It is best to do this in a formulation that preserves spin rotation invariance at all stages, and this is facilitated by the coherent state path integral (see Chap. 13 of [49]). The essential structure of this path integral can be understood simply by looking at a single spin in a magnetic field $\mathbf{h}$ with the Hamiltonian $H_1 = -\mathbf{h} \cdot \mathbf{S}$. Then its partition function at a temperature T is given by

$$\mathrm{Tr} \exp\left(\mathbf{h} \cdot \mathbf{S}/T\right) = \int \mathcal{D}\mathbf{n}(\tau) \exp\left(i2S\mathcal{A}[\mathbf{n}(\tau)] + S \int_0^{1/T} d\tau \mathbf{h} \cdot \mathbf{n}(\tau) \right). \tag{9.30}$$

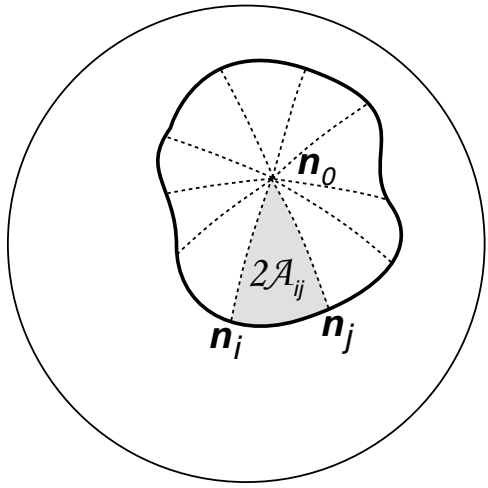

Fig. 9.7. The path traced out by a single spin on the unit sphere in imaginary time. After discretizing time, the area enclose by the path is written as the sum over the areas of spherical triangles: $\mathcal{A}_{ij}$ is half the area of the triangle with vertices $\mathbf{n}_0$, $\mathbf{n}_i$, $\mathbf{n}_j$. Different choices for the arbitrary point $\mathbf{n}_0$ correspond to different gauge choices associated with (9.32) and (9.34).

Here S is the angular momentum of the spin $\mathbf{S}$ (we are interested primarily in the case $S = 1/2$) and $\mathbf{n}(\tau)$ is a unit 3-vector with $\mathbf{n}(0) = \mathbf{n}(1/T)$. So the above path integral is over all closed curves on the surface of a sphere. The first term in the action of the path integral is the crucial Berry phase: $\mathcal{A}[\mathbf{n}(\tau)]$ is *half* the oriented area enclosed by the curve $\mathbf{n}(\tau)$ (the reason for the half will become clear momentarily). Note that this area is only defined modulo 4π, the surface area of a unit sphere. The expression (9.30) has an obvious generalization to the lattice Hamiltonian H_s: the action adds up the Berry phases of every spin, and there is an additional energy term which is just the Hamiltonian with the replacement $\mathbf{S}_j \to S\mathbf{n}_j$.

We are now faced with the problem of keeping track of the areas enclosed by the curves traced out by all the spins. This seems rather daunting, particularly because the half-area $\mathcal{A}[\mathbf{n}(\tau)]$ is a global object defined by the whole curve, and cannot be obviously be associated with local portions of the curve. One convenient way to proceed is illustrated in Fig. 9.7: discretize imaginary time, choose a fixed arbitrary point $\mathbf{n}_0$ on the sphere, and thus write the area as the sum of a large number of spherical triangles. Note that each triangle is associated with a local portion of the curve $\mathbf{n}(\tau)$.

We now need an expression for $\mathcal{A}(\mathbf{n}_1, \mathbf{n}_2, \mathbf{n}_3)$, defined as half the area of the spherical triangle with vertices $\mathbf{n}_1$, $\mathbf{n}_2$, $\mathbf{n}_3$. Complicated expressions for this appear in treatises on spherical trigonometry, but a far simpler expression is obtained after transforming to spinor variables [50]. Let us write

$$\mathbf{n}_j \equiv z_{ja}^* \boldsymbol{\sigma}_{ab} z_{jb}, \tag{9.31}$$

where $a, b = \uparrow, \downarrow$ and we will always assume an implied summation over such indices, $\boldsymbol{\sigma}_{ab}$ are the Pauli matrices, and $z_{j\uparrow}$, $z_{j\downarrow}$ are complex numbers obeying $|z_{j\uparrow}|^2 + |z_{j\downarrow}|^2 = 1$. Note that knowledge of $\mathbf{n}_j$ only defines z_{ja} up to a U(1) gauge transformation under which

$$z_{ja} \to z_{ja} e^{i\phi_j}. \tag{9.32}$$

Then, associated with each pair of vertices $\mathbf{n}_i, \mathbf{n}_j$ we define

$$\mathcal{A}_{ij} \equiv \arg\left[z_{ia}^* z_{ja}\right]. \tag{9.33}$$

Under the gauge transformation (9.32) we have

$$\mathcal{A}_{ij} \to \mathcal{A}_{ij} - \phi_i + \phi_j, \tag{9.34}$$

i.e. $\mathcal{A}_{ij}$ behaves like a U(1) gauge field. Note also that $\mathcal{A}_{ij}$ is only defined modulo 2π, and that $\mathcal{A}_{ji} = -\mathcal{A}_{ij}$. For future use, we also mention the following identity, which follows from (9.31) and (9.33):

$$z_{ia}^* z_{ja} = \left(\frac{1 + \mathbf{n}_i \cdot \mathbf{n}_j}{2}\right)^{1/2} e^{i\mathcal{A}_{ij}}. \tag{9.35}$$

The classical result for the half-area of the spherical triangle can be written in the simple form in terms of the present U(1) gauge variables:

$$\mathcal{A}(\mathbf{n}_1, \mathbf{n}_2, \mathbf{n}_3) = \mathcal{A}_{12} + \mathcal{A}_{23} + \mathcal{A}_{31}. \tag{9.36}$$

We chose $\mathcal{A}$ as a *half*-area earlier mainly because then the expressions (9.33) and (9.36) come out without numerical factors. It is satisfying to observe that this total area is invariant under (9.34), and that the half-area is ambiguous modulo 2π.

Using (9.36), we can now write down a useful expression for $\mathcal{A}[\mathbf{n}(\tau)]$. We assume that imaginary time is discretized into times τ_j separated by intervals $\Delta\tau$. Also, we denote by $j+\tau$ the site at time $\tau_j + \Delta\tau$, and define $\mathcal{A}_{j,j+\tau} \equiv \mathcal{A}_{j\tau}$. Then

$$\mathcal{A}[\mathbf{n}(\tau)] = \sum_j \mathcal{A}_{j\tau}. \tag{9.37}$$

Note that this expression is a gauge-invariant function of the U(1) gauge field $\mathcal{A}_{j\tau}$, and is analogous to the quantity sometimes called the Polyakov loop.

We are now ready to write down the first form proposed effective action for the quantum fluctuating Néel state. We do need to address some simple book-keeping considerations first:
(i) Discretize spacetime into a cubic lattice of points j. Note that the same index j referred to points along imaginary time above, and to square lattice

points in H_s. The meaning of the site index should be clear from the context.
(*ii*) On each spacetime point j, we represent quantum spin operator $\mathbf{S}_j$ by

$$\mathbf{S}_j = \eta_j S \mathbf{n}_j, \tag{9.38}$$

where $\mathbf{n}_j$ is a unit vector, and $\eta_j = \pm 1$ is the sublattice staggering factor appearing in (9.2). This representation is that expected from the coherent state path integral, apart from the η_j factor. We have chosen to include η_j because of the expected local antiferromagnetic correlations of the spins. So in a quantum fluctuating Néel state, we can reasonably expect $\mathbf{n}_j$ to be a slowly varying function of j.
(*iii*) Associated with each $\mathbf{n}_j$, define a spinor z_{ja} by (9.31).
(*iv*) With each link of the cubic lattice, we use (9.33) to associate with it a $\mathcal{A}_{j\mu} \equiv \mathcal{A}_{j,j+\mu}$. Here $\mu = x, y, \tau$ extends over the 3 spacetime directions.
With these preliminaries in hand, we can motivate the following effective action for fluctuations under the Hamiltonian H_s:

$$\widetilde{\mathcal{Z}} = \prod_{ja} \int dz_{ja} \prod_j \delta\left(|z_{ja}|^2 - 1\right) \exp\left(\tfrac{1}{\widetilde{g}} \sum_{\langle ij \rangle} \mathbf{n}_i \cdot \mathbf{n}_j + i2S \sum_j \eta_j \mathcal{A}_{j\tau}\right). \tag{9.39}$$

Here the summation over $\langle ij \rangle$ extends over nearest neighbors on the cubic lattice. The integrals are over the z_{ja}, and the $\mathbf{n}_j$ and $\mathcal{A}_{j\tau}$ are *dependent* variables defined via (9.31) and (9.33). Note that both terms in the action are invariant under the gauge transformation (9.32); consequently, we could equally well have rewritten $\widetilde{\mathcal{Z}}$ as an integral over the $\mathbf{n}_j$, but it turns out to be more convenient to use the z_{ja} and to integrate over the redundant gauge degree of freedom. The first term in the action contains the energy of the Hamiltonian H_s, and acts to prefer nearest neighbor $\mathbf{n}_j$ which are parallel to each other—this "ferromagnetic" coupling between the $\mathbf{n}_j$ in spacetime ensures, via (9.38), that the local quantum spin configurations are as in the Néel state. The second term in the action is simply the Berry phase required in the coherent state path integral, as obtained from (9.30) and (9.37): the additional factor of η_j compensates for that in (9.38). The dimensionless coupling $\widetilde{g}$ controls the strength of the local antiferromagnetic correlations; it is like a "temperature" for the ferromagnet in spacetime. So for small $\widetilde{g}$ we expect $\widetilde{\mathcal{Z}}$ to be in the Néel phase, while for large $\widetilde{g}$ we can expect a quantum-"disordered" paramagnet. For a much more careful derivation of the partition function $\widetilde{\mathcal{Z}}$ from the underlying antiferromagnet H_s, including a quantitative estimate of the value of $\widetilde{g}$, see *e.g.* Chap. 13 of [49].

While it is possible to proceed with the remaining analysis of this section using $\widetilde{\mathcal{Z}}$, we find it more convenient to work with a very closely related alternative model. Our proposed theory for the quantum fluctuating antiferromagnet in its final form is [51, 52]

$$\mathcal{Z} = \prod_{j\mu} \int_0^{2\pi} \frac{dA_{j\mu}}{2\pi} \prod_{ja} \int dz_{ja} \prod_j \delta\left(|z_{ja}|^2 - 1\right) \exp\left(\frac{1}{g} \sum_{j\mu} \left(z_{ja}^* e^{-iA_{j\mu}} z_{j+\mu,a} + \text{c.c.}\right) + i2S \sum_j \eta_j A_{j\tau}\right). \tag{9.40}$$

Note that we have introduced a new field $A_{j\mu}$, on each link of the cubic lattice, which is integrated over. Like $\mathcal{A}_{i\mu}$, this is also a U(1) gauge field because all terms in the action above are invariant under the analog of (9.34):

$$A_{j\mu} \to A_{j\mu} - \phi_j + \phi_{j+\mu}. \tag{9.41}$$

The very close relationship between $\mathcal{Z}$ and $\widetilde{\mathcal{Z}}$ may be seen [51] by explicitly integrating over the $A_{j\mu}$ in (9.40): this integral can be done exactly because the integrand factorizes into terms on each link that depend only on a single $A_{j\mu}$. After inserting (9.35) into (9.40), the integral over the $j\mu$ link is

$$\int_0^{2\pi} \frac{dA_{j\mu}}{2\pi} \exp\left(\frac{(2(1+\mathbf{n}_j \cdot \mathbf{n}_{j+\mu}))^{1/2}}{g} \cos(\mathcal{A}_{j\mu} - A_{j\mu}) + i2S\eta_j \delta_{\mu\tau} A_{j\mu}\right) = I_{2S\delta_{\mu\tau}} \left[\frac{(2(1+\mathbf{n}_j \cdot \mathbf{n}_{j+\mu}))^{1/2}}{g}\right] \exp\left(i2S\eta_j \delta_{\mu\tau} \mathcal{A}_{j\mu}\right), \tag{9.42}$$

where the result involves either the modified Bessel function I_0 (for $\mu = x, y$) or I_{2S} (for $\mu = \tau$). We can use the identity (9.42) to perform the integral over $A_{j\mu}$ on each link of (9.40), and so obtain a partition function, denoted $\mathcal{Z}'$, as an integral over the z_{ja} only. This partition function $\mathcal{Z}'$ has essentially the same structure as $\widetilde{\mathcal{Z}}$ in (9.39). The Berry phase term in $\mathcal{Z}'$ is identical to that in $\widetilde{\mathcal{Z}}$. The integrand of $\mathcal{Z}'$ also contains a real action expressed solely as a sum over functions of $\mathbf{n}_i \cdot \mathbf{n}_j$ on nearest neighbor links: in $\widetilde{\mathcal{Z}}$ this function is simply $\mathbf{n}_i \cdot \mathbf{n}_j / \widetilde{g}$, but the corresponding function obtained from (9.40) is more complicated (it involves the logarithm of a Bessel function), and has distinct forms on spatial and temporal links. We do not expect this detailed form of the real action function to be of particular importance for universal properties: the initial simple nearest-neighbor ferromagnetic coupling between the $\mathbf{n}_j$ in (9.39) was chosen arbitrarily anyway. So we may safely work with the theory $\mathcal{Z}$ in (9.40) henceforth.

One of the important advantages of (9.40) is that we no longer have to keep track of the complicated non-linear constraints associated with (9.31) and (9.33); this was one of the undesirable features of (9.39). In $\mathcal{Z}$, we simply have free integration over the independent variables z_{ja} and $A_{j\mu}$. The remainder of this section will be devoted to describing the properties of $\mathcal{Z}$ as a function of the coupling g.

The theory $\mathcal{Z}$ in (9.40) has some resemblance to the so-called CP^{N-1} model from the particle physics literature [50, 53, 54]: our indices a, b take only 2 possible values, but the general model is obtained when $a, b = 1 \ldots N$, and we will also find it useful to consider $\mathcal{Z}$ for general N. The case of general N describes SU(N) and Sp(N) antiferromagnets on the square lattice [19]. Note also that it is essential for our purposes that the theory is invariant under $A_{j\mu} \to A_{j\mu} + 2\pi$, and so the U(1) gauge theory is *compact*. Finally our model contains a Berry phase term (which can be interpreted as a $J_\mu A_\mu$ term associated with a current $J_{j\mu} = 2S\eta_j \delta_{\mu\tau}$ of static charges $\pm 2S$ on each site) which is not present in any of the particle physics analyses. This Berry phase term will be an essential central actor in all of our results below for the paramagnetic phase and the quantum phase transition.

The properties of $\mathcal{Z}$ are quite evident in the limit of small g. Here, the partition function is strongly dominated by configurations in which the real part of the action is a minimum. In a suitable gauge, these are the configurations in which z_{ja} = constant, and by (9.31), we also have $\mathbf{n}_j$ a constant. This obviously corresponds to the Néel phase with (9.2). A Gaussian fluctuation analysis about such a constant saddle point is easily performed, and we obtain the expected spectrum of a doublet of gapless spin waves.

The situation is much more complicated for large g where we should naturally expect a paramagnetic phase with $\langle \mathbf{S}_j \rangle = \langle \mathbf{n}_j \rangle = 0$. This will be discussed in some detail in Sect. 9.4.1. Finally, we will address the nature of the quantum phase transition between the Néel and paramagnetic phases in Sect. 9.4.2.

9.4.1 Paramagnetic Phase

The discussion in this section has been adapted from another recent review by the author [55].

For large g, we can perform the analog of a 'high temperature' expansion of $\mathcal{Z}$ in (9.40). We expand the integrand in powers of $1/g$ and perform the integral over the z_{ja} term-by-term. The result is then an effective theory for the compact U(1) gauge field $A_{j\mu}$ alone. An explicit expression for the effective action of this theory can be obtained in powers of $1/g$: this has the structure of a strong coupling expansion in lattice gauge theory, and higher powers of $1/g$ yield terms dependent upon gauge-invariant U(1) fluxes on loops of all sizes residing on the links of the cubic lattice. For our purposes, it is sufficient to retain only the simplest such term on elementary square plaquettes, yielding the partition function

$$\widetilde{\mathcal{Z}}_A = \prod_{j\mu} \int_0^{2\pi} \frac{dA_{j\mu}}{2\pi} \exp\left(\frac{1}{e^2} \sum_{\square} \cos\left(\epsilon_{\mu\nu\lambda} \Delta_\nu A_{j\lambda}\right) - i2S \sum_j \eta_j A_{j\tau} \right), \tag{9.43}$$

where $\epsilon_{\mu\nu\lambda}$ is the totally antisymmetric tensor in three spacetime dimensions. Here the cosine term represents the conventional Maxwell action for a compact U(1) gauge theory: it is the simplest local term consistent with the gauge symmetry (9.41) and which is periodic under $A_{j\mu} \to A_{j\mu} + 2\pi$; closely related terms appear under the $1/g$ expansion. The sum over $\Box$ in (9.43) extends over all plaquettes of the cubic lattice, Δ_μ is the standard discrete lattice derivative ($\Delta_\mu f_j \equiv f_{j+\mu} - f_j$ for any f_j), and e^2 is a coupling constant. We expect the value of e to increase monotonically with g.

As is standard in duality mappings, we first rewrite the partition function in $2+1$ spacetime dimensions by replacing the cosine interaction in (9.43) by a Villain sum [56, 57] over periodic Gaussians:

$$\mathcal{Z}_A = \sum_{\{q_{\bar{j}\mu}\}} \prod_{j\mu} \int_0^{2\pi} \frac{dA_{j\mu}}{2\pi} \exp\Bigg(-\frac{1}{2e^2} \sum_{\Box} \left(\epsilon_{\mu\nu\lambda}\Delta_\nu A_{j\lambda} - 2\pi q_{\bar{j}\mu}\right)^2 - i2S \sum_j \eta_j A_{j\tau} \Bigg), \tag{9.44}$$

where the $q_{\bar{j}\mu}$ are integers on the links of the *dual* cubic lattice, which pierce the plaquettes of the direct lattice. Throughout this article we will use the index $\bar{j}$ to refer to sites of this dual lattice, while j refers to the direct lattice on sites on which the spins are located.

We will now perform a series of exact manipulations on (9.44) which will lead to a dual *interface* model [19, 20, 58]. This dual model has only positive weights—this fact, of course, makes it much more amenable to a standard statistical analysis. This first step in the duality transformation is to rewrite (9.44) by the Poisson summation formula:

$$\sum_{\{q_{\bar{j}\mu}\}} \exp\ \left(-\frac{1}{2e^2} \sum_{\Box} \left(\epsilon_{\mu\nu\lambda}\Delta_\nu A_{j\lambda} - 2\pi q_{\bar{j}\mu}\right)^2 \right) = \sum_{\{a_{\bar{j}\mu}\}} \exp\left(-\frac{e^2}{2} \sum_{\bar{j}} a_{\bar{j}\mu}^2 - i \sum_{\Box} \epsilon_{\mu\nu\lambda} a_{\bar{j}\mu} \Delta_\nu A_{j\lambda} \right) \tag{9.45}$$

where $a_{\bar{j}\mu}$ (like $q_{\bar{j}\mu}$) is an integer-valued vector field on the links of the dual lattice (here, and below, we drop overall normalization factors in front of the partition function). Next, we write the Berry phase in a form more amenable to duality transformations. Choose a 'background' $a_{\bar{j}\mu} = a^0_{\bar{j}\mu}$ flux which satisfies

$$\epsilon_{\mu\nu\lambda}\Delta_\nu a^0_{\bar{j}\lambda} = \eta_j \delta_{\mu\tau}, \tag{9.46}$$

where j is the direct lattice site in the center of the plaquette defined by the curl on the left-hand-side. Any integer-valued solution of (9.46) is an acceptable choice for $a^0_{\bar{j}\mu}$, and a convenient choice is shown in Fig. 9.8. Using

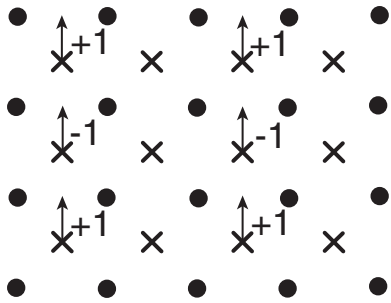

Fig. 9.8. Specification of the non-zero values of the fixed field $a^0_{\bar{j}\mu}$. The circles are the sites of the direct lattice, j, while the crosses are the sites of the dual lattice, $\bar{j}$; the latter are also offset by half a lattice spacing in the direction out of the paper (the $\mu = \tau$ direction). The $a^0_{\bar{j}\mu}$ are all zero for $\mu = \tau, x$, while the only non-zero values of $a^0_{\bar{j}y}$ are shown above. Notice that the a^0 flux obeys (9.46).

(9.46) to rewrite the Berry phase in (9.44), applying (9.45), and shifting $a_{\bar{j}\mu}$ by the integer $2Sa^0_{\bar{j}\mu}$, we obtain a new exact representation of $\mathcal{Z}_A$ in (9.44):

$$\mathcal{Z}_A = \sum_{\{a_{\bar{j}\mu}\}} \prod_{j\mu} \int_0^{2\pi} \frac{dA_{j\mu}}{2\pi} \exp\left(-\frac{e^2}{2} \sum_{\bar{j},\mu} (a_{\bar{j}\mu} - 2Sa^0_{\bar{j}\mu})^2 \right.$$
$$\left. -i \sum_{\square} \epsilon_{\mu\nu\lambda} a_{\bar{j}\mu} \Delta_\nu A_{j\lambda} \right). \quad (9.47)$$

The integral over the $A_{j\mu}$ can be performed independently on each link, and its only consequence is the imposition of the constraint $\epsilon_{\mu\nu\lambda}\Delta_\nu a_{\bar{j}\lambda} = 0$. We solve this constraint by writing $a_{\bar{j}\mu}$ as the gradient of an integer-valued 'height' $h_{\bar{j}}$ on the sites of the dual lattice, and so obtain

$$\mathcal{Z}_h = \sum_{\{h_{\bar{j}}\}} \exp\left(-\frac{e^2}{2} \sum_{\bar{j},\mu} (\Delta_\mu h_{\bar{j}} - 2Sa^0_{\bar{j}\mu})^2 \right). \quad (9.48)$$

We emphasize that, apart from an overall normalization, we have $\mathcal{Z}_h = \mathcal{Z}_A$ exactly. This is the promised 2+1 dimensional interface, or height, model in almost its final form.

The physical properties of (9.48) become clearer by converting the "frustration" $a^0_{\bar{j}\mu}$ in (9.48) into offsets for the allowed height values. This is done by decomposing $a^0_{\bar{j}\mu}$ into curl and divergence free parts and writing it in terms of new fixed fields, $\mathcal{X}_{\bar{j}}$ and $\mathcal{Y}_{j\mu}$ as follows:

$$a^0_{\bar{j}\mu} = \Delta_\mu \mathcal{X}_{\bar{j}} + \epsilon_{\mu\nu\lambda}\Delta_\nu \mathcal{Y}_{j\lambda}. \quad (9.49)$$

The values of these new fields are shown in Fig. 9.9. Inserting (9.49) into (9.48), we can now write the height model in its simplest form [20]

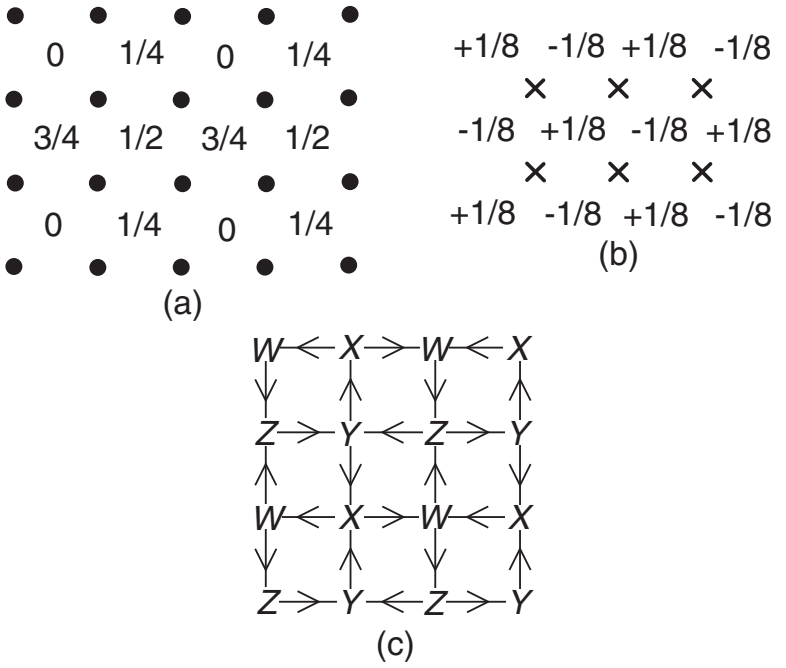

Fig. 9.9. Specification of the non-zero values of the fixed fields (a) $\mathcal{X}_{\bar{\jmath}}$, (b) $\mathcal{Y}_{j\mu}$, (c) $\epsilon_{\mu\nu\lambda}\Delta_\nu\mathcal{Y}_{j\lambda}$ introduced in (9.49). The notational conventions are as in Fig. 9.8. Only the $\mu = \tau$ components of $\mathcal{Y}_{j\mu}$ are non-zero, and these are shown in (b). Only the spatial components of $\epsilon_{\mu\nu\lambda}\Delta_\nu\mathcal{Y}_{j\lambda}$ are non-zero, and these are oriented as in (c) with magnitude 1/4. The four dual sublattices, W, X, Y, Z, are also indicated in (c). Note that $\mathcal{X}_W = 0$, $\mathcal{X}_X = 1/4$, $\mathcal{X}_Y = 1/2$, and $\mathcal{X}_Z = 3/4$.

$$\mathcal{Z}_h = \sum_{\{H_{\bar{\jmath}}\}} \exp\left(-\frac{e^2}{2}\sum_{\bar{\jmath}}(\Delta_\mu H_{\bar{\jmath}})^2\right), \tag{9.50}$$

where

$$H_{\bar{\jmath}} \equiv h_{\bar{\jmath}} - 2S\mathcal{X}_{\bar{\jmath}} \tag{9.51}$$

is the new height variable we shall work with. Notice that the $\mathcal{Y}_{j\mu}$ have dropped out, while the $\mathcal{X}_{\bar{\jmath}}$ act only as fractional offsets (for S not an even integer) to the integer heights. From (9.51) we see that for half-odd-integer S the height is restricted to be an integer on one of the four sublattices, an integer plus 1/4 on the second, an integer plus 1/2 on the third, and an integer plus 3/4 on the fourth; the fractional parts of these heights are as shown in Fig. 9.9a; the steps between neighboring heights are always an integer plus 1/4, or an integer plus 3/4. For S an odd integer, the heights are integers on one square sublattice, and half-odd-integers on the second sublattice. Finally

for even integer S the offset has no effect and the height is an integer on all sites. We discuss these classes of S values in turn in the following subsections.

4.1.1 S Even Integer

In this case the offsets $2S\mathcal{X}_{\bar{\jmath}}$ are all integers, and (9.50) is just an ordinary three dimensional height model which has been much studied in the literature [57,59]. Unlike the two-dimensional case, three-dimensional height models generically have no roughening transition, and the interface is always smooth [59]. With all heights integers, the smooth phase breaks no lattice symmetries. So square lattice antiferromagnets with S even integer can have a paramagnetic ground state with a spin gap and no broken symmetries. The smooth interface corresponds to confinement in the dual compact U(1) gauge theory [60]: consequently the z_a of $\mathcal{Z}$ are confined, and the elementary excitations are $S = 1$ quasiparticles, similar to the φ_α of $\mathcal{S}_\varphi$. This is in accord with the exact ground state for a $S = 2$ antiferromagnet on the square lattice found by Affleck *et al.*, the AKLT state [61].

4.1.2 S Half-Odd-Integer

Now the heights of the interface model can take four possible values, which are integers plus the offsets on the four square sublattices shown in Fig. 9.9a. As in Sect. 9.4.1.1, the interface is always smooth *i.e.* any state of (9.50) has a fixed average interface height

$$\overline{H} \equiv \frac{1}{N_d} \sum_{\bar{\jmath}=1}^{N_d} \langle H_{\bar{\jmath}} \rangle, \tag{9.52}$$

where the sum is over a large set of N_d dual lattice points which respect the square lattice symmetry. *Any* well-defined value for $\overline{H}$ breaks the uniform shift symmetry of the height model under which $H_{\bar{\jmath}} \to H_{\bar{\jmath}} \pm 1$. In the present context, only the value of $\overline{H}$ modulo integers is physically significant, and so the breaking of the shift symmetry is not important by itself. However, after accounting for the height offsets, we now prove that *any smooth interface must also break a lattice symmetry with the development of bond order*: this means that $\mathcal{Z}_A$ in (9.44) describes spin gap ground states of the lattice antiferromagnet which necessarily have spontaneous bond order.

The proof of this central result becomes clear upon a careful study of the manner in which the height model in (9.50) and (9.51) implements the 90° rotation symmetry about a direct square lattice point. Consider such a rotation under which the dual sublattice points in Fig. 9.9c interchange as

$$W \to X, \quad X \to Y, \quad Y \to Z, \quad Z \to W. \tag{9.53}$$

The terms in the action in (9.51) will undergo a 90° rotation under this transformation provided the integer heights $h_{\bar{\jmath}}$ transform as

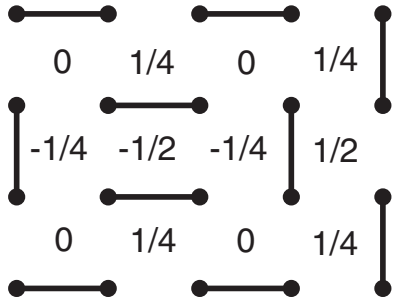

Fig. 9.10. Mapping between the quantum dimer model and the interface model $\mathcal{Z}_h$ in (9.50). Each dimer on the direct lattice is associated with a step in height of $\pm 3/4$ on the link of the dual lattice that crosses it. All other height steps are $\pm 1/4$. Each dimer represents a singlet valence bond between the sites, as in Fig. 9.2.

$$h_W \to h_X, \quad h_X \to h_Y, \quad h_Y \to h_Z, \quad h_Z \to h_W - 1. \tag{9.54}$$

Notice the all important -1 in the last term—this compensates for the 'branch cut' in the values of the offsets $\mathcal{X}_{\vec{\jmath}}$ as one goes around a plaquette in Fig. 9.9c. From (9.54), it is evident that the average height $\overline{H} \to \overline{H} - 1/4$ under the 90° rotation symmetry under consideration here. Hence, a smooth interface with a well-defined value of $\overline{H}$ *always* breaks this symmetry.

We now make this somewhat abstract discussion more physical by presenting a simple interpretation of the interface model in the language of the $S = 1/2$ antiferromagnet [62]. From Fig. 9.9a it is clear that nearest neighbor heights can differ either by $1/4$ or $3/4$ (modulo integers). To minimize the action in (9.50), we should choose the interface with the largest possible number of steps of $\pm 1/4$. However, the interface is frustrated, and it is not possible to make all steps $\pm 1/4$ and at least a quarter of the steps must be $\pm 3/4$. Indeed, there is a precise one-to-one mapping between interfaces with the minimal number of $\pm 3/4$ steps (we regard interfaces differing by a uniform integer shift in all heights as equivalent) and the dimer coverings of the square lattice: the proof of this claim is illustrated in Fig. 9.10. We identify each dimer with a singlet valence bond between the spins (the ellipses in Fig. 9.2), and so each interface corresponds to a quantum state with each spin locked in a singlet valence bond with a particular nearest neighbor. Fluctuations of the interface in imaginary time between such configurations correspond to quantum tunneling events between such dimer states, and an effective Hamiltonian for this is provided by the quantum dimer model [63]. While such an interpretation in terms of the dimer model is appealing, we should also note that it is not as general as the dual interface model: on certain lattices, while the collinear paramagnetic state continues to have a representation as a dual interface model, there is no corresponding dimer interpretation [64].

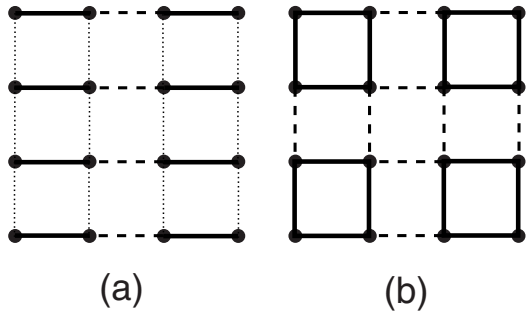

Fig. 9.11. Sketch of the two simplest possible states with bond order for $S = 1/2$ on the square lattice: (a) the columnar spin-Peierls states, and (b) plaquette state. Here the distinct line styles encode the different values of the bond order parameter Q_{ij} in (9.29) on the links. This should be contrasted from Figs. 9.1–9.4 where the line styles represented distinct values of the exchange constants in the Hamiltonian. In the present section, the Hamiltonian has the full symmetry of the square lattice, and the orderings represented above amount to a spontaneous breaking of the lattice symmetry. Both states above are 4-fold degenerate; an 8-fold degenerate state, with superposition of the above orders, also appears as a possible ground state of the generalized interface model. Numerical studies of a number of two-dimensional quantum antiferromagnets [66–68, 70, 73–75] have found ground states with spontaneous bond order, similar to the states shown above.

The nature of the possible smooth phases of the interface model are easy to determine from the above picture and by standard techniques from statistical theory [20, 62]. As a simple example, the above mapping between interface heights and dimer coverings allows one to deduce that interfaces with average height $\overline{H} = 1/8, 3/8, 5/8, 7/8$ (modulo integers) correspond to the four-fold degenerate bond-ordered states in Fig. 9.11a. To see this, select the interface with $h_{\bar{\jmath}} = 0$ for all $\bar{\jmath}$: this interface has the same symmetry as Fig. 9.11a, and a simple computation summing over sites from (9.51) shows that this state has average height $\overline{H} = -(0 + 1/4 + 1/2 + 3/4)/4 = -3/8$ for $S = 1/2$. The remaining three values of $\overline{H}$ correspond to the three other states obtained by successive 90° rotations of Fig. 9.11a. In a similar manner, interfaces with $\overline{H} = 0, 1/4, 1/2, 3/4$ (modulo integers) correspond to the four-fold degenerate plaquette bond-ordered states in Fig. 9.11b. A simple example of such an interface is the "disordered-flat" state [65] in which $h_{\bar{\jmath}} = 0$ on all sites $\bar{\jmath}$, except for the W sublattice which have $\mathcal{X}_{\bar{\jmath}} = 0$; for these sites we have $h_{\bar{\jmath}}$ fluctuate randomly between $h_{\bar{\jmath}} = 0$ and $h_{\bar{\jmath}} = 1$, and independently for different $\bar{\jmath}$. The average height of such an interface is $\overline{H} = -((0+1)/2+1/4+1/2+3/4)/4 = -1/2$ for $S = 1/2$, and the mapping to dimer coverings in Fig. 9.10 shows easily that such an interface corresponds to the state in Fig. 9.11b. All values of $\overline{H}$ other than those quoted above are associated with eight-fold degenerate bond-ordered states with a superposition of the orders in Fig. 9.11a and b.

All these phases are expected to support non-zero spin quasiparticle excitations which carry spin $S = 1$, but not $S = 1/2$. Despite the local corrugation in the interface configuration introduced by the offsets, the interface remains smooth on the average, and this continues to correspond to confinement in the dual compact U(1) gauge theory [60]. Consequently the spinons of Fig. 9.3b are confined in pairs. The structure of the resulting $S = 1$ triplon quasiparticles is very similar to the excitations of the paramagnetic phase of the coupled dimer antiferromagnet of Sect. 9.2, as we already noted in Sect. 9.1.

Support for the class of bond-ordered states described above has appeared in a number of numerical studies of $S = 1/2$ antiferromagnets in $d = 2$ which have succeeded in moving from the small g Néel phase to the large g paramagnet. These include studies on the honeycomb lattice [66] (duality mapping on the honeycomb lattice appears in [19]), on the planar pyrochlore lattice [67,68] (duality mapping for a lattice with the symmetry of the planar pyrochlore is in [64, 69], with a prediction for the bond order observed), on square lattice models with ring-exchange and easy-plane spin symmetry [70] (duality mapping on spin models with easy plane symmetry is in [52, 71, 72]), and square lattice models with SU(N) symmetry [73] (the theories (9.40), with $a = 1 \ldots N$, and (9.50) apply unchanged to SU(N) antiferromagnets). The case of the square lattice antiferromagnet with first and second neighbor exchange is not conclusively settled: while two recent studies [74, 75] (and earlier work [25,76]) do observe bond order in a paramagnetic spin-gap state, a third [77] has so far not found such order. It is possible that this last study is observing signatures of the critical point between the Néel and bond-ordered states (to be described in Sect. 9.4.2) which is expressed in a theory for deconfined spinons in $\mathcal{Z}_c$ in (9.55).

Finally, we also mention that evidence for the spontaneous bond order of Fig. 9.11 appears in recent numerical studies of *doped* antiferromagnets [78, 79].

4.1.3 S Odd Integer

This case is similar to that S half-odd-integer, and we will not consider it in detail. The Berry phases again induce bond order in the spin gap state, but this order need only lead to a two-fold degeneracy.

9.4.2 Critical Theory

We turn finally to the very difficult issue of the nature of the quantum phase transition from the Néel state to one of the bond-ordered paramagnetic states in Fig. 9.10 as a function of increasing g. This has been a long-standing open problem, and many different proposals have been made. The two phases break different symmetries of the Hamiltonian, and so are characterized by very different order parameters (one lives in spin space, and the other in real

space). Landau-Ginzburg-Wilson (LGW) theory would imply that a generic second-order transition is not possible between such phases, and one obtains either a first-order transition or a region of co-existence of the two orders. However, the bond-order in the paramagnet was obtained entirely from quantum Berry phases attached to the fluctuating Néel order, and it is not clear that LGW theory applies in such a situation.

Recent work by Senthil *et al.* [80, 81] has proposed an elegant resolution to many of these problems, and we will describe their results in the remainder of this subsection. The results are based upon solutions of a series of simpler models which strongly suggest that related results also apply to the SU(2) invariant, $S = 1/2$ models of interest. The computations are intricate, but the final results are quite easy to state, and are presented below. We will mainly limit our discussion here to the case of antiferromagnets of spin $S = 1/2$.

First, contrary to the predictions of LGW theory, a generic second-order transition between the Néel state and the bond-ordered paramagnet is indeed possible (let us assume it occurs at $g = g_c$ for $\mathcal{Z}$ in (9.40)). The theory for such a quantum critical point is obtained simply by taking a naive continuum limit of $\mathcal{Z}$ while ignoring *both* the compactness of the gauge field and the Berry phases. Remarkably, these complications of the lattice model $\mathcal{Z}$, which we have so far stated were essential for the complete theory, have effects which cancel each other out, but *only* at the critical point. Note compactness on its own is a relevant perturbation which cannot be ignored *i.e.* without Berry phases, the compact and non-compact lattice CP^1 model have distinct critical theories [82]. However, the surprising new point noted by Senthil *et al.* [80, 81] is that the *non-compact CP^1 model has the same critical theory as the compact CP^1 model with $S = 1/2$ Berry phases.* Taking the naive continuum limit of $\mathcal{Z}$ in (9.40), and softening the hard-constraint on the z_{ja}, we obtain the proposed theory for the quantum critical point between the Néel state and the bond-ordered paramagnet for spin $S = 1/2$ [80, 81]:

$$\mathcal{Z}_c = \int \mathcal{D}z_a(r,\tau)\mathcal{D}A_\mu(r,\tau)\exp\left(-\int d^2r d\tau\left[|(\partial_\mu - iA_\mu)z_a|^2 + s|z_a|^2 + \frac{u}{2}(|z_a|^2)^2 + \frac{1}{4e^2}(\epsilon_{\mu\nu\lambda}\partial_\nu A_\lambda)^2\right]\right). \tag{9.55}$$

We have also included here a kinetic term for the A_μ, and one can imagine that this is generated by integrating out large momentum z_{ja}. On its own, $\mathcal{Z}_c$ describes the transition from a magnetically ordered phase with z_a condensed at $s < s_c$, to a disordered state with a gapless U(1) photon at $s > s_c$ (here s_c is the critical point of $\mathcal{Z}_c$). Clearly the $s < s_c$ phase corresponds to the Néel phase of $\mathcal{Z}$ in (9.40) for $g < g_c$. However, the $s > s_c$ phase does not obviously correspond to the $g > g_c$ bond-ordered, fully gapped, paramagnet of $\mathcal{Z}$. This is repaired by accounting for the compactness of the gauge field

and the Berry phases: it is no longer possible to neglect them, while it was safe to do so precisely at $g = g_c$. The *combined* effects of compactness and Berry phases are therefore *dangerously irrelevant* at $g = g_c$.

It is important to note that the critical theory of (9.55) is distinct from the critical theory $\mathcal{S}_\varphi$ in (9.12), although both theories have a global O(3) symmetry [82]. In particular the values of the exponents ν are different in the two theories, and the scaling dimension of the Néel order parameter φ_α under $\mathcal{S}_\varphi$ is distinct from the scaling dimension of the Néel order parameter $z_a^* \sigma_{ab}^\alpha z_b$ at the critical point of $\mathcal{Z}_c$.

It is interesting that $\mathcal{Z}_c$ in (9.55) is a theory for the $S = 1/2$ spinors z_a. These can be understood to be the continuum realization of the spinons shown earlier in Fig. 9.3b. Thus the spinons become the proper elementary degrees of freedom, but *only* at the quantum critical point. Hence it is appropriate to label this as a 'deconfined quantum critical point' [80]. These spinons are confined into a $S = 1$ quasiparticle once bond order appears for $g > g_c$, for reasons similar to those illustrated in Fig. 9.3b.

A key characteristic of this 'deconfined' critical point is the irrelevance of the compactness of the gauge field, and hence of monopole tunnelling events. A consequence of this is that the flux of the A_μ gauge field in $\mathcal{Z}_c$ is conserved. This emergent conservation law, and the associated long-range gauge forces are key characteristics of such critical points.

We summarize in Fig. 9.12 our results for $S = 1/2$ square lattice antiferromagnets, as described by $\mathcal{Z}$ in (9.40).

The claims above for the conspiracy between the compactness and Berry phases at the critical point are surprising and new. They are central to a complete understanding of square lattice antiferromagnets, and a full justification of the claims appears in the work of Senthil *et al.*. The following subsections illustrate their origin by considering a series of models, of increasing complexity, where similar phenomena can be shown to occur. The reader may also find it useful to look ahead to Tables 1 and 2, which summarize the intricate relationships between the models considered.

4.2.1 Lattice Model at $N = 1$

This subsection describes a simplified lattice gauge theory model introduced by Sachdev and Jalabert [51]. While the duality analysis presented below was initiated in [51], its correct physical interpretation, and the implications for more general models are due to Senthil *et al.* [80, 81].

The model of interest in this subsection is the $N = 1$ case of $\mathcal{Z}$. Physically, such a model will be appropriate for an antiferromagnet in the presence of a staggered magnetic field: such a field will prefer $z_\uparrow$ over $z_\downarrow$ (say). So we write the preferred single component complex scalar simply as $z_j = e^{i\theta_j}$, and obtain from (9.40)

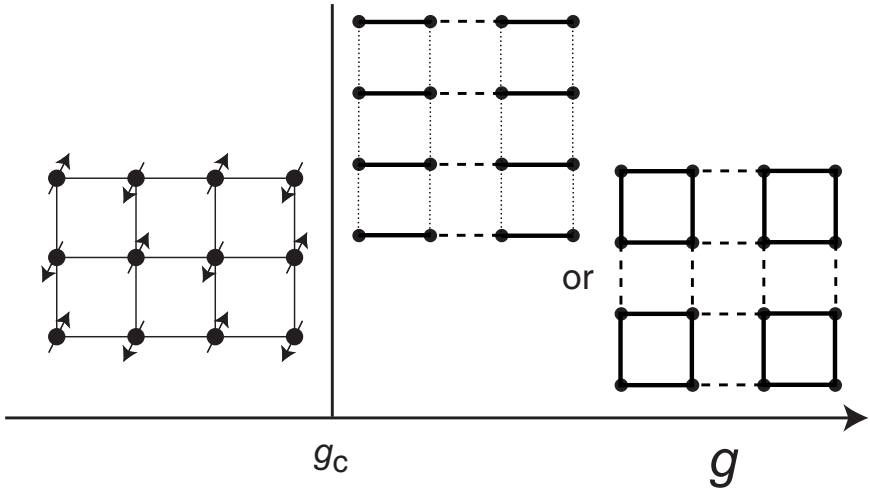

Fig. 9.12. Phase diagram of the model $\mathcal{Z}$ in (9.40) of $S = 1/2$ antiferromagnets with full square lattice symmetry. There is a Néel phase for $g < g_c$ which breaks spin rotation invariance; it has a doublet of gapless spin wave excitations. The bond-ordered paramagnet for $g > g_c$ preserves spin rotation invariance but breaks square lattice symmetry; it has a gap to all excitations, and the non-zero spin excitations are described by $S = 1$ triplet quasiparticles which are very similar to the 'triplons' discussed in Sect. 9.2.1. The critical point at $g = g_c$ is described by the theory of $S = 1/2$ 'spinons', $\mathcal{Z}_c$ in (9.55) at its critical point $s = s_c$; note that this mapping to the spinon theory $\mathcal{Z}_c$ does not work away from $g = g_c$, and spinons are confined for all $g > g_c$. A phase diagram like the one above has been used as a point of departure to obtain a phase diagram for doped Mott insulators [22, 83], as a description of the cuprate superconductors; evidence for spontaneous bond order in doped antiferromagnets appears in [78, 79].

$$\mathcal{Z}_1 = \prod_j \int_0^{2\pi} \frac{d\theta_j}{2\pi} \int_0^{2\pi} \frac{dA_{j\mu}}{2\pi} \exp\left(\frac{1}{e^2} \sum_{\square} \cos\left(\epsilon_{\mu\nu\lambda} \Delta_\nu A_{j\lambda}\right) + \frac{1}{g} \sum_{j,\mu} \cos\left(\Delta_\mu \theta_j - A_{j\mu}\right) + i2S \sum_j \eta_j A_{j\tau} \right). \quad (9.56)$$

We have chosen here to explicitly include a compact Maxwell term for the gauge field, as that proves convenient in the description of the duality mappings. Note that if we integrate out the θ_j for large g, then we again obtain the model $\mathcal{Z}_A$ in (9.43) which was used to describe the paramagnetic phase in Sect. 9.4.1. So bond order appears also in the model $\mathcal{Z}_1$ at large g. This bond order disappears as g is reduced, at a transition we will describe below.

Rather than attack $\mathcal{Z}_1$ directly, it is useful as a warm-up, and to make contact with previous work, to consider a sequence of simpler models that

have been considered in the literature. As we have emphasized, $\mathcal{Z}_1$ features the combined complications of compactness and Berry phases, essential for a proper description of quantum antiferromagnets. It is the simplest model in which it can be shown that these complications effectively neutralize one another at the critical point.

In the following subsection, we make things simpler for ourselves momentarily by dropping *both* the compactness and the Berry phases. We will then, in the subsequent subsections, add these complications back in.

A. XY Model with a Non-compact U(1) Gauge Field

Dropping both compactness and Berry phases, $\mathcal{Z}_1$ reduces to

$$\mathcal{Z}_{\rm SC} = \prod_j \int_0^{2\pi} \frac{d\theta_j}{2\pi} \int_{-\infty}^{\infty} dA_{j\mu} \exp\left(-\frac{1}{2e^2} \sum_{\Box} \left(\epsilon_{\mu\nu\lambda} \Delta_\nu A_{j\lambda}\right)^2 + \frac{1}{g} \sum_{j,\mu} \cos\left(\Delta_\mu \theta_j - A_{j\mu}\right) \right). \quad (9.57)$$

Notice that the Maxwell term for the gauge field now has a simple Gaussian form. This is simply the lattice, classical, Ginzburg-Landau model (or an XY model) of a superconductor at finite temperatures coupled to electromagnetism. This model has been studied extensively in the past, and the key result was provided by Dasgupta and Halperin [84]. As we review below, they showed that $\mathcal{Z}_{\rm SC}$ exhibited an *inverted XY transition* *i.e.* it was dual to the theory of a complex scalar ψ in the absence of a gauge field:

$$\mathcal{Z}_{\rm SC,dual} = \int \mathcal{D}\psi(r,\tau) \exp\left(-\int d^2 r d\tau \left(|\partial_\mu \psi|^2 + \overline{s}|\psi|^2 + \frac{\overline{u}}{2}|\psi|^4 \right) \right). \quad (9.58)$$

The field ψ is a creation operator for *vortices* in the original theory of the Ginzburg-Landau superconductor. These have a short-range interaction ($\overline{u}$ above) because of the screening provided by the electromagnetic flux quantum attached to every vortex in (9.57). So the vortex loops of (9.57) behave like the world lines of the dual boson field of (9.58). The tuning parameter $\overline{s}$ in (9.58) is 'inverted' from the perspective of the direct theory: the $\overline{s} < \overline{s}_c$ phase with $\langle\psi\rangle \neq 0$ has a vortex condensate and so is the normal state of a Ginzburg-Landau superconductor, while the $\overline{s} > \overline{s}_c$ phase with $\langle\psi\rangle = 0$ has the vortices gapped as in the superconducting phase.

We now provide a few steps in the analysis which links (9.57) to (9.58). The steps are very similar to those described in Sect. 9.4.1 below (9.43) and (9.44). We write the cosine in (9.57) in its Villain form, decouple it by the Poisson summation formula using integer currents $J_{j\mu}$, and also decouple the Maxwell term by a Hubbard-Stratonovich field $P_{\bar{j}\mu}$; this yields the analog of (9.45) for $\mathcal{Z}_{\rm SC}$:

$$\mathcal{Z}_{\rm SC,1} = \prod_j \int_0^{2\pi} \frac{d\theta_j}{2\pi} \int_{-\infty}^{\infty} dA_{j\mu} \sum_{\{J_{j\mu}\}} \int_{-\infty}^{\infty} dP_{\bar{j}\mu} \exp\left(-\frac{e^2}{2} \sum_{\bar{j},\mu} P_{\bar{j}\mu}^2 \right.$$
$$\left. -\frac{g}{2} \sum_{j\mu} J_{j\mu}^2 + i \sum_j J_{j\mu} \left(\Delta_\mu \theta_j - A_{j\mu} \right) + i \sum_{\Box} \epsilon_{\mu\nu\lambda} P_{\bar{j}\mu} \Delta_\nu A_{j\lambda} \right). \quad (9.59)$$

The advantage of this form is that the integrals over θ_j and $A_{j\mu}$ can be performed exactly, and they lead to the constraints

$$\Delta_\mu J_{j\mu} = 0 \quad ; \quad J_{j\mu} = \epsilon_{\mu\nu\lambda} \Delta_\nu P_{\bar{j}\lambda}. \quad (9.60)$$

We solve these constraints by writing

$$J_{j\mu} = \epsilon_{\mu\nu\lambda} \Delta_\nu b_{\bar{j}\lambda} \quad ; \quad P_{\bar{j}\mu} = b_{\bar{j}\mu} - \Delta_\mu \varphi_{\bar{j}}, \quad (9.61)$$

where $b_{\bar{j}\mu}$ is an integer valued field on the links of the dual lattice, and $\varphi_{\bar{j}}$ is a real valued field on the sites of the dual lattice. This transforms (9.59) to

$$\mathcal{Z}_{\rm SC,2} = \prod_{\bar{j}} \int_{-\infty}^{\infty} d\varphi_{\bar{j}} \sum_{\{b_{\bar{j}\mu}\}} \exp\left(-\frac{e^2}{2} \sum_{\bar{j},\mu} \left(b_{\bar{j}\mu} - \Delta_\mu \varphi_{\bar{j}} \right)^2 \right.$$
$$\left. -\frac{g}{2} \sum_{\Box} \left(\epsilon_{\mu\nu\lambda} \Delta_\nu b_{\bar{j}\lambda} \right)^2 \right); \quad (9.62)$$

precisely this dual form was obtained by Dasgupta and Halperin [84], and used by them for numerical simulations. We proceed further analytically, using methods familiar in the theory of duality mappings [57]: we promote the integer valued $b_{\bar{j}\mu}$ to a real field by the Poisson summation method, and introduce, by hand, a vortex fugacity y_v. This transforms $\mathcal{Z}_{\rm SC,2}$ to

$$\mathcal{Z}_{\rm SC,3} = \prod_{\bar{j}} \int_{-\infty}^{\infty} db_{\bar{j}\mu} \int_{-\infty}^{\infty} d\varphi_{\bar{j}} \int_{-\infty}^{\infty} d\vartheta_{\bar{j}} \exp\left(-\frac{e^2}{2} \sum_{\bar{j},\mu} \left(b_{\bar{j}\mu} - \Delta_\mu \varphi_{\bar{j}} \right)^2 \right.$$
$$\left. -\frac{g}{2} \sum_{\Box} \left(\epsilon_{\mu\nu\lambda} \Delta_\nu b_{\bar{j}\lambda} \right)^2 + y_v \sum_{\bar{j},\mu} \cos\left(2\pi b_{\bar{j}\mu} - \Delta_\mu \vartheta_{\bar{j}} \right) \right). \quad (9.63)$$

Notice that the effect of the vortex fugacity is to yield the least action when $b_{\bar{j}\mu}$ is an integer (ignore $\vartheta_{\bar{j}}$ momentarily): so we have effectively 'softened' the integer constraint on $b_{\bar{j}\mu}$. We have also introduced here a new real valued field $\vartheta_{\bar{j}}$ on the sites of the dual lattice simply to make the $\mathcal{Z}_{\rm SC,3}$ invariant under U(1) gauge transformations of $b_{\bar{j}\mu}$. This is mainly because the physics is clearer in this explicitly gauge-invariant form. We could, if we had wished, also chosen a gauge in which $\vartheta_{\bar{j}} = 0$, and then the field $\vartheta_{\bar{j}}$ would not be present in $\mathcal{Z}_{\rm SC,3}$ (this justifies neglect of $\vartheta_{\bar{j}}$ above). In the complete form in (9.63), it is clear from the first two Gaussian terms that fluctuations of the $b_{\bar{j}\mu}$ gauge

field have been 'Higgsed' by the real field $\varphi_{\bar{\jmath}}$. Indeed, it is more convenient to choose a gauge in which $\varphi_{\bar{\jmath}} = 0$, and we do so. Now the fluctuations of $b_{\bar{\jmath}\mu}$ are 'massive' and so can be safely integrated out. To leading order in y_v, this involves simply replacing $b_{\bar{\jmath}\mu}$ with the saddle point value obtained from the first two Gaussian terms, which is $\overline{b}_{\bar{\jmath}\mu} = 0$. So we have the very simple final theory

$$\mathcal{Z}_{\mathrm{SC},4} = \prod_{\bar{\jmath}} \int_{-\infty}^{\infty} d\vartheta_{\bar{\jmath}} \exp\left(y_v \sum_{\bar{\jmath},\mu} \cos\left(\Delta_\mu \vartheta_{\bar{\jmath}}\right) \right), \tag{9.64}$$

which has the form of the dual XY model. We now take the continuum limit of (9.64) by a standard procedure [85] of introducing a complex field ψ conjugate to $e^{i\vartheta_{\bar{\jmath}}}$, and obtain the theory $\mathcal{Z}_{\mathrm{SC,dual}}$ as promised. This establishes the duality mapping of Dasgupta and Halperin [84].

B. XY Model with a Compact U(1) Gauge Field

Now we ease towards our aim of a duality analysis of $\mathcal{Z}_1$, by adding one layer of complexity to $\mathcal{Z}_{\mathrm{SC}}$. We make the gauge field in (9.57) compact by including a cosine Maxwell term [86]:

$$\mathcal{Z}_M = \prod_j \int_0^{2\pi} \frac{d\theta_j}{2\pi} \int_0^{2\pi} \frac{dA_{j\mu}}{2\pi} \exp\left(\frac{1}{e^2} \sum_{\square} \cos\left(\epsilon_{\mu\nu\lambda} \Delta_\nu A_{j\lambda}\right) + \frac{1}{g} \sum_{j,\mu} \cos\left(\Delta_\mu \theta_j - A_{j\mu}\right) \right). \tag{9.65}$$

The Dasgupta-Halperin duality mapping can be easily extended to this theory. We now write both cosine terms in their Villain forms, and then proceed as described above. The results (9.59) and (9.62) continue to have the same form, with the only change being that the fields $P_{\bar{\jmath}\mu}$ and $\varphi_{\bar{\jmath}}$ are now also *integer* valued (and so must be summed over). Promoting these integer valued fields to real fields by the Poisson summation method following [57], we now have to introduce *two* fugacities: a vortex fugacity y_v (as before), and a monopole fugacity $\tilde{y}_m$ (discussed below). Consequently, $\mathcal{Z}_{\mathrm{SC},3}$ in (9.63) now takes the form

$$\mathcal{Z}_{M,3} = \prod_{\bar{\jmath}} \int_{-\infty}^{\infty} db_{\bar{\jmath}\mu} \int_{-\infty}^{\infty} d\varphi_{\bar{\jmath}} \int_{-\infty}^{\infty} d\vartheta_{\bar{\jmath}} \exp\left(-\frac{e^2}{2} \sum_{\bar{\jmath},\mu} \left(b_{\bar{\jmath}\mu} - \Delta_\mu \varphi_{\bar{\jmath}}\right)^2 - \frac{g}{2} \sum_{\square} \left(\epsilon_{\mu\nu\lambda} \Delta_\nu b_{\bar{\jmath}\lambda}\right)^2 + y_v \sum_{\bar{\jmath},\mu} \cos\left(2\pi b_{\bar{\jmath}\mu} - \Delta_\mu \vartheta_{\bar{\jmath}}\right) + \tilde{y}_m \sum_{\bar{\jmath}} \cos\left(2\pi \varphi_{\bar{\jmath}} - \vartheta_{\bar{\jmath}}\right) \right). \tag{9.66}$$

Again, the positions of the $\vartheta_{\bar{\jmath}}$ above are dictated by gauge invariance, and the effect of the vortex and monopole fugacities is to soften the integer value constraints on the $b_{\bar{\jmath}\mu}$ and $\varphi_{\bar{\jmath}}$. Proceeding as described below (9.63), we work in the gauge $\varphi_{\bar{\jmath}} = 0$, and to leading order in y_v, $\tilde{y}_m$ replace $b_{\bar{\jmath}\mu}$ by its saddle point value in the Gaussian part of the action, which remains $\bar{b}_{\bar{\jmath}\mu} = 0$. Then, instead of (9.64), we obtain

$$\mathcal{Z}_{M,4} = \prod_{\bar{\jmath}} \int_{-\infty}^{\infty} d\vartheta_{\bar{\jmath}} \exp\left(y_v \sum_{\bar{\jmath},\mu} \cos\left(\Delta_\mu \vartheta_{\bar{\jmath}}\right) + \tilde{y}_m \sum_{\bar{\jmath}} \cos\left(\vartheta_{\bar{\jmath}}\right) \right). \tag{9.67}$$

We see that the new second term in (9.67) acts like an ordering field on the dual XY model. Taking the continuum limit as was done below (9.64) using [85] a complex field ψ conjugate to $e^{i\vartheta_{\bar{\jmath}}}$, now instead of $\mathcal{Z}_{\mathrm{SC,dual}}$ in (9.58) we obtain [87, 88]

$$\mathcal{Z}_{M,\mathrm{dual}} = \int \mathcal{D}\psi(r,\tau) \exp\Bigg(- \int d^2 r d\tau \Bigg(|\partial_\mu \psi|^2 + \overline{s}|\psi|^2 + \frac{\overline{u}}{2}|\psi|^4 - y_m(\psi + \psi^*) \Bigg) \Bigg). \tag{9.68}$$

The new term proportional to y_m has the interpretation of a *monopole fugacity*. The compact gauge field now permits Dirac monopoles, which are points in spacetime at which vortex loops of the 'superconductor' can end: hence y_m is coupled to the creation and annihilation operators for the dual boson ψ *i.e.* the vortices. In the form (9.68) it is also clear that y_m acts like an ordering field in the dual XY model. We expect that such an XY model has no phase transition, and $\langle\psi\rangle \neq 0$ for all $\overline{s}$. So the presence of monopoles has destroyed the 'superconducting' phase. Comparing the properties of (9.58) and (9.68) we therefore conclude that making the gauge field compact in $\mathcal{Z}_{\mathrm{SC}}$ in (9.57) is a strongly relevant perturbation: the inverted XY transition of $\mathcal{Z}_{\mathrm{SC}}$ is destroyed in the resulting model $\mathcal{Z}_M$.

C. Berry Phases

We are finally ready to face $\mathcal{Z}_1$, and add in the final layer of complication of the Berry phases. Again, the Dasgupta-Halperin duality can be extended by combining it with the methods of Sect. 9.4.1 (this was partly discussed in [51]). Now the monopoles carry Berry phases [19, 89], and these lead to cancellations among many monopole configurations. In the long-wavelength limit it turns out that the only important configurations are those in which the total monopole magnetic charge is q times the charge of the elementary monopole [19, 20, 89]. Here q is the smallest positive integer such that

$$e^{i\pi Sq} = 1, \tag{9.69}$$

i.e. $q = 4$ for S half an odd integer, $q = 2$ for S an odd integer, and $q = 1$ for S an even integer. Using the physical interpretation of (9.68), we therefore conclude that the monopole fugacity term should be replaced by one in which the monopoles are created and annihilated in multiples of q; the dual theory of $\mathcal{Z}_1$ in (9.56) then becomes

$$\mathcal{Z}_{1,\mathrm{dual}} = \int \mathcal{D}\psi(r,\tau) \exp\Bigg(- \int d^2 r d\tau \Bigg(|\partial_\mu \psi|^2 + \overline{s}|\psi|^2 + \frac{\overline{u}}{2}|\psi|^4 - y_{mq}(\psi^q + \psi^{*q}) \Bigg) \Bigg). \tag{9.70}$$

An explicit derivation of the mapping from $\mathcal{Z}_1$ to $\mathcal{Z}_{1,\mathrm{dual}}$ can be obtained by an extension of the methods described above for $\mathcal{Z}_{\mathrm{SC}}$ and $\mathcal{Z}_M$. We express the Berry phase term using the 'background field' $a^0_{\bar{\jmath}\mu}$ in (9.46), and then we find that $\mathcal{Z}_{\mathrm{SC},2}$ in (9.62) is now replaced by

$$\mathcal{Z}_{1,2} = \sum_{\{b_{\bar{\jmath}\mu}\}} \sum_{\{\varphi_{\bar{\jmath}}\}} \exp\left(-\frac{e^2}{2} \sum_{\bar{\jmath},\mu} \left(b_{\bar{\jmath}\mu} - \Delta_\mu \varphi_{\bar{\jmath}} - 2S a^0_{\bar{\jmath}\mu} \right)^2 - \frac{g}{2} \sum_{\square} \left(\epsilon_{\mu\nu\lambda} \Delta_\nu b_{\bar{\jmath}\lambda} \right)^2 \right). \tag{9.71}$$

Notice that, as in Sect. 9.4.1, the Berry phases appear as offsets in the dual action. We now promote the integer field $b_{\bar{\jmath}\mu}$ and $\varphi_{\bar{\jmath}}$ to real fields by the Poisson summation method (just as in (9.66)), at the cost of introducing vortex and monopole fugacities. The final steps, following the procedure below (9.66), are to transform to the gauge $\varphi_{\bar{\jmath}} = 0$, and to then set the 'Higgsed' dual gauge field $b_{\bar{\jmath}\mu}$ to its saddle point value determined from the Gaussian terms in the action. It is the latter step which is now different, and the presence of the $a^0_{\bar{\jmath}\mu}$ now implies that the saddle point value $\overline{b}_{\bar{\jmath}\mu}$ will be non-zero and site dependent. Indeed, it is crucial that the saddle point be determined with great care, and that the square lattice symmetry of the underlying problem be fully respected. This saddle point determination is in many ways analogous to the computation in Sect. III.B of [20], and it is important that all the modes on the lattice scale be fully identified in a similar manner. The similarity to [20] becomes clear after using the parameterization in (9.49) for $a^0_{\bar{\jmath}\mu}$ in terms of the $\mathcal{X}_{\bar{\jmath}}$ and the $\mathcal{Y}_{j\mu}$ shown in Fig. 9.9. Finally, after transforming $b_{\bar{\jmath}\mu} \to b_{\bar{\jmath}\mu} + 2S\Delta_\mu \mathcal{X}_{\bar{\jmath}}$ and $\vartheta_{\bar{\jmath}} \to \vartheta_{\bar{\jmath}} + 4\pi S \mathcal{X}_{\bar{\jmath}}$, we obtain from (9.71)

$$\mathcal{Z}_{1,3} = \prod_{\bar{\jmath}} \int_{-\infty}^{\infty} db_{\bar{\jmath}\mu} \int_{-\infty}^{\infty} d\vartheta_{\bar{\jmath}} \exp\left(-\frac{e^2}{2} \sum_{\bar{\jmath},\mu} \left(b_{\bar{\jmath}\mu} - 2S\epsilon_{\mu\nu\lambda} \Delta_\nu \mathcal{Y}_\lambda \right)^2 \right.$$
$$- \frac{g}{2} \sum_{\square} \left(\epsilon_{\mu\nu\lambda} \Delta_\nu b_{\bar{\jmath}\lambda} \right)^2 + y_v \sum_{\bar{\jmath},\mu} \cos\left(2\pi b_{\bar{\jmath}\mu} - \Delta_\mu \vartheta_{\bar{\jmath}} \right)$$
$$\left. + \tilde{y}_m \sum_{\bar{\jmath}} \cos\left(\vartheta_{\bar{\jmath}} + 4\pi S \mathcal{X}_{\bar{\jmath}} \right) \right). \tag{9.72}$$

Now, the saddle point value of the massive field $b_{\bar{\jmath}\mu}$ is easily determined from the first terms in (9.72), yielding

$$\bar{b}_{\bar{\jmath}\mu} = \alpha \epsilon_{\mu\nu\lambda} \Delta_\nu \mathcal{Y}_{j\lambda}. \tag{9.73}$$

where $\alpha \equiv 2Se^2/(e^2 + 8g)$. Note that only the spatial components of $\bar{b}_{\bar{\jmath}\mu}$ are non-zero, and these have the simple structure of Fig. 9.9c. In particular, the magnitude of the $\bar{b}_{\bar{\jmath}\mu}$ are the same on all the spatial links, and the use of (9.49) was crucial in obtaining this appealing result. With this saddle point value, (9.72) simplifies to the following model for the field $\vartheta_{\bar{\jmath}}$ only (this is the form of (9.67) after accounting for Berry phases):

$$\mathcal{Z}_{1,4} = \prod_{\bar{\jmath}} \int_{-\infty}^{\infty} d\vartheta_{\bar{\jmath}} \exp\left(y_v \sum_{\bar{\jmath},\mu} \cos\left(\Delta_\mu \vartheta_{\bar{\jmath}} - 2\pi \bar{b}_{\bar{\jmath}\mu} \right) \right.$$
$$\left. + \tilde{y}_m \sum_{\bar{\jmath}} \cos\left(\vartheta_{\bar{\jmath}} + 4\pi S \mathcal{X}_{\bar{\jmath}} \right) \right). \tag{9.74}$$

The most important property of this dual XY model is the nature of the ordering field in the last term of (9.74). For $S = 1/2$, notice from Fig. 9.9a that this field is oriented north/east/south/west on the four sublattices in of the dual lattice in Fig. 9.9c. So if we take a naive continuum limit, the average field vanishes! This is the key effect responsible for the cancellations among monopole configurations induced by Berry phases noted earlier; in the dual formulation, the Berry phases have appeared in differing orientations of the dual ordering field. The XY model in (9.74) also has the contribution from $\bar{b}_{\bar{\jmath}\mu}$, which appear as a 'staggered flux' acting on the $\vartheta_{\bar{\jmath}}$ (see Fig. 9.9c), but we now show that this is not as crucial in the continuum limit.

Before we take the continuum limit of $\mathcal{Z}_{1,4}$, we discuss its implementation of the square lattice symmetries. In particular, we are interested in the Z_4 symmetry which rotates the four sublattices in Fig. 9.9c into each other, as the values of $\mathcal{X}_{\bar{\jmath}}$ seem to distinguish between them. Let us consider the symmetry $\mathcal{R}_n$ which rotates lattice anticlockwise by an angle $n\pi/2$ about the direct lattice point at the center of a plaquette in Fig. 9.9c, associated with the transformation in (9.53). It is easy to see that $\mathcal{Z}_{1,4}$ remains invariant under $\mathcal{R}_n$ provided we simultaneously rotate the angular variables $\vartheta_{\bar{\jmath}}$:

$$\mathcal{R}_n : \quad \vartheta_{\bar{\jmath}} \to \vartheta_{\bar{\jmath}} + nS\pi. \tag{9.75}$$

It is now useful to introduce complex variables which realize irreducible representations of this Z_4 symmetry. We divide the lattice into plaquettes like those in Fig. 9.9c, and for each plaquette we define variables ψ_p, with p integer, by

$$\psi_p = \frac{1}{2}\left(e^{i\vartheta_W} + e^{ip\pi/2}e^{i\vartheta_X} + e^{ip\pi}e^{i\vartheta_Y} + e^{i3p\pi/2}e^{i\vartheta_Z}\right). \tag{9.76}$$

Note that we need only use $p = 0, 1, 2, 3$ because ψ_p depends only on $p(\mathrm{mod}\ 4)$. Under the symmetry $\mathcal{R}_n$ we clearly have

$$\mathcal{R}_n : \quad \psi_p \to e^{in(2S-p)\pi/2}\psi_p; \tag{9.77}$$

the factor of $e^{inS\pi}$ arises from (9.75), and that of $e^{-inp\pi/2}$ from the real-space rotation of the lattice points. Note that only for $p = 2S$ is ψ_p invariant under $\mathcal{R}_n$, and this is consistent with the fact that it is ψ_{2S} which appears in $\mathcal{Z}_{1,4}$ as the ordering field term. Let us now write the action in $\mathcal{Z}_{1,4}$ in terms of these new variables. Ignoring the spacetime variation from plaquette to plaquette, the action per plaquette is

$$\mathcal{S}_{1,4} = -2y_v \sum_{p=0}^{3}\left[\cos\left(\pi(p-\alpha)/2\right)|\psi_p|^2\right] - \tilde{y}_m\left(\psi_{2S} + \psi_{2S}^*\right) + \ldots \tag{9.78}$$

Here the ellipses represent other allowed terms, all consistent with the symmetry (9.77), which must be included to implement the (softened) constraints on ψ_p arising from (9.76) and the fact that the $e^{i\vartheta_{\bar{\jmath}}}$ are unimodular. Apart from ψ_{2S}, for which there is already an ordering field in the action, the condensation of any of the other ψ_p breaks the lattice symmetry (9.77), and so drives a quantum phase transition to the bond-ordered state. The choice among the ψ_p is controlled by the coefficient of the y_v term in (9.78), and we choose the value of $p \neq 2S$ for which $\cos\left(\pi(\alpha+p)/2\right)$ is a maximum. We are interested in the large g paramagnetic phase, and here α is small, and the appropriate value is $p = 0$. The resulting continuum theory for $\psi = \psi_0$ then must be invariant under (9.77), and it is easily seen that this has just the form $\mathcal{Z}_{1,\mathrm{dual}}$ in (9.70) with q determined by (9.69). Other choices of p for the order parameter lead to different types of bond order, with a ground state degeneracy smaller or larger than the q in (9.69); such states have partial or additional bond order, and are clearly possible in general. However, our analysis of the paramagnetic states in Sect. 9.4.1 indicates that a choice $\psi = \psi_{p\neq 0}$ is unlikely for the models under consideration here, and we will not consider this case further here.

We have now completed our promised derivation of the model $\mathcal{Z}_{1,\mathrm{dual}}$ in (9.70) dual to the $N = 1$ lattice gauge theory model $\mathcal{Z}_1$ in (9.56). Rather than being an XY model in a field (as in (9.68)), $\mathcal{Z}_{1,\mathrm{dual}}$ is an XY model with a q-fold anisotropy. This anisotropy encapsulates the q-fold binding of monopoles claimed earlier. In the language of (9.74) the average ordering

Table 9.1. Summary of the duality mappings for $N = 1$. Only the Lagrangean's are specified, and a summation/integration of these over spacetimes is implicit. The fixed field $\eta_j = \pm 1$ in the Berry phase in the third row is the sublattice staggering factor in (9.2). The integer q in the third row is specified in (9.69). For $S = 1/2$, we have $q = 4$, and then the y_{mq} perturbation is dangerously irrelevant. Hence the critical theory for the model with monopoles and Berry phases in the third row, is identical to that for the first row

$N = 1$	
Direct lattice model	**Dual model**
$\mathcal{L}_{SC} = (1/(2e^2))\,(\epsilon_{\mu\nu\lambda}\Delta_\nu A_{j\lambda})^2 - (1/g)\cos(\Delta_\mu\theta_j - A_{j\mu})$	$\mathcal{L}_{SC,\mathrm{dual}} = \lvert\partial_\mu\psi\rvert^2 + \overline{s}\lvert\psi\rvert^2 + \frac{\overline{u}}{2}\lvert\psi\rvert^4$
$\mathcal{L}_M = -(1/e^2)\cos(\epsilon_{\mu\nu\lambda}\Delta_\nu A_{j\lambda}) - (1/g)\cos(\Delta_\mu\theta_j - A_{j\mu})$	$\mathcal{L}_{M,\mathrm{dual}} = \lvert\partial_\mu\psi\rvert^2 + \overline{s}\lvert\psi\rvert^2 + \frac{\overline{u}}{2}\lvert\psi\rvert^4 - y_m(\psi + \psi^*)$
$\mathcal{L}_1 = -(1/e^2)\cos(\epsilon_{\mu\nu\lambda}\Delta_\nu A_{j\lambda}) - (1/g)\cos(\Delta_\mu\theta_j - A_{j\mu}) - i2S\eta_j A_{j\tau}$	$\mathcal{L}_{1,\mathrm{dual}} = \lvert\partial_\mu\psi\rvert^2 + \overline{s}\lvert\psi\rvert^2 + \frac{\overline{u}}{2}\lvert\psi\rvert^4 - y_{mq}(\psi^q + \psi^{*q})$

fields on the $\vartheta_{\bar{\jmath}}$ oscillate from site to site and cancel out, and only the q-th moment of the field survives. Now the combined effect of the monopoles and Berry phases in $\mathcal{Z}_1$ is decided by the term proportional to y_{mq}. In the paramagnetic phase of the direct model, which is $\overline{s} < \overline{s}_c$ and $\langle\psi\rangle \neq 0$, this q-fold anisotropy is certainly very important. For $S = 1/2$, $q = 4$ it orders the ψ field along four particular angles, and these are easily shown to be [51] one of the four degenerate bond-ordered states in Fig. 9.11. However, at the critical point $\overline{s} = \overline{s}_c$ it is known that this 4-fold anisotropy is irrelevant [90]: so in $\mathcal{Z}_{1,\mathrm{dual}}$ the monopoles can be neglected at the critical point $s = s_c$, but not away from it.

We have now achieved the desired objective of this subsection. Compactness alone was a strongly relevant perturbation on the model of a scalar field coupled to electromagnetism in $\mathcal{Z}_{\mathrm{SC}}$. However, when we combined compactness with the Berry phases in $\mathcal{Z}_1$, then we found that the monopoles effectively cancelled each other out at the critical point for $S = 1/2$. Consequently the

theory for the critical point in $\mathcal{Z}_1$ is identical to the theory for the critical point in $\mathcal{Z}_{\rm SC}$, and this is the simple inverted XY model $\mathcal{Z}_{\rm SC,dual}$ in (9.58). The results of this subsection are summarized in Table 1.

4.2.2 Easy Plane Model at $N = 2$

A second explicit example of the remarkable phenomenon described above is provided by the physically relevant $N = 2$ case of the model of central interest, $\mathcal{Z}$ in (9.40), but in the presence of an additional spin-anisotropy term preferring that the spins lie within the XY plane. In such a situation, we may write the complex spinor z_{ja} as

$$z_{ja} = \frac{1}{\sqrt{2}} \begin{pmatrix} e^{i\theta_{j\uparrow}} \\ e^{i\theta_{j\downarrow}} \end{pmatrix}, \tag{9.79}$$

so that the action is expressed in terms of *two* angular fields, $\theta_\uparrow$ and $\theta_\downarrow$. Inserting (9.79) in (9.40), we obtain a generalization of the $N = 1$ model $\mathcal{Z}_1$ in (9.56):

$$\mathcal{Z}_2 = \prod_j \int_0^{2\pi} \frac{d\theta_{j\uparrow}}{2\pi} \int_0^{2\pi} \frac{d\theta_{j\downarrow}}{2\pi} \int_0^{2\pi} \frac{dA_{j\mu}}{2\pi} \exp\left(\frac{1}{e^2} \sum_\square \cos\left(\epsilon_{\mu\nu\lambda} \Delta_\nu A_{j\lambda}\right) \right.$$
$$\left. + \frac{1}{2g} \sum_{j,\mu,a} \cos\left(\Delta_\mu \theta_{ja} - A_{j\mu}\right) + i2S \sum_j \eta_j A_{j\tau} \right). \tag{9.80}$$

As in (9.56), we have chosen to explicitly include a Maxwell term for the U(1) gauge field as it proves convenient in the subsequent duality analysis. The model $\mathcal{Z}_2$ provides a complete description of the phases of the square lattice antiferromagnet (9.28) with an additional easy-plane anisotropy term.

We can now proceed with a duality analysis of (9.80) using methods precisely analogous to those discussed in Sect. 9.4.2.1: the only difference is we now have two angular fields $\theta_{a=\uparrow,\downarrow}$, and so certain fields come with two copies. We will therefore not present any details, and simply state the series of results which appear here, which closely parallel those obtained above for $N = 1$.

- Neglecting *both* compactness of the $U(1)$ gauge field and the Berry phases, it is straightforward to take the continuum limit of $\mathcal{Z}_2$ in its direct representation, and we obtain the theory $\mathcal{Z}_c$ in (9.55), but with an additional spin-anisotropy term

$$\mathcal{Z}_{2c} = \int \mathcal{D}z_a(r,\tau)\mathcal{D}A_\mu(r,\tau) \exp\left(- \int d^2r d\tau \left[|(\partial_\mu - iA_\mu)z_a|^2 + s|z_a|^2 \right.\right.$$
$$\left.\left. + \frac{u}{2}(|z_a|^2)^2 + v|z_\uparrow|^2|z_\downarrow|^2 + \frac{1}{4e^2}(\epsilon_{\mu\nu\lambda}\partial_\nu A_\lambda)^2 \right] \right), \tag{9.81}$$

where $v > 0$ prefers spins in the easy plane. We can carry through the analog of the duality mapping between (9.57) and (9.58), and instead of (9.58) we now obtain a theory for *two* dual fields ψ_a representing vortices in $\theta_\uparrow$ and $\theta_\downarrow$ [82]

$$\mathcal{Z}_{2c,\mathrm{dual}} = \int \mathcal{D}\psi_a(r,\tau)\mathcal{D}B_\mu(r,\tau)\exp\left(-\int d^2r d\tau\left[|(\partial_\mu - iB_\mu)\psi_\uparrow|^2 + |(\partial_\mu + iB_\mu)\psi_\downarrow|^2 + \overline{s}|\psi_a|^2 + \frac{\overline{u}}{2}(|\psi_a|^2)^2 + \overline{v}|\psi_\uparrow|^2|\psi_\downarrow|^2 + \frac{1}{4\overline{e}^2}(\epsilon_{\mu\nu\lambda}\partial_\nu B_\lambda)^2\right]\right). \tag{9.82}$$

Note that there is now a non-compact U(1) gauge field B_μ which survives the continuum limit: this field arises from the analog of the field $b_{\bar{j}\mu}$ in (9.63), and here it is not completely Higgsed out. The most remarkable property of (9.82) is that it is identical in structure to (9.81): the actions are identical under the mapping $z_\uparrow \to \psi_\uparrow$, $z_\downarrow \to \psi^*_\downarrow$, and $A_\mu \to B_\mu$. In other words, the theory $\mathcal{Z}_{2c}$ is *self-dual* [82].

- As in Sect. 9.4.2.1, we next make the A_μ gauge field compact, but continue to ignore Berry phases *i.e.* we perform a duality analysis on (9.80), in the absence of the last term in the action. Now, instead of (9.68), (9.82) is modified to

$$\mathcal{Z}_{2M,\mathrm{dual}} = \int \mathcal{D}\psi_a(r,\tau)\mathcal{D}B_\mu(r,\tau)\exp\left(-\int d^2r d\tau\left[|(\partial_\mu - iB_\mu)\psi_\uparrow|^2 + |(\partial_\mu + iB_\mu)\psi_\downarrow|^2 + \overline{s}|\psi_a|^2 + \frac{\overline{u}}{2}(|\psi_a|^2)^2 + \overline{v}|\psi_\uparrow|^2|\psi_\downarrow|^2 + \frac{1}{4\overline{e}^2}(\epsilon_{\mu\nu\lambda}\partial_\nu B_\lambda)^2 - y_m(\psi_\uparrow\psi_\downarrow + \psi^*_\downarrow\psi^*_\uparrow)\right]\right). \tag{9.83}$$

The last term represents the influence of monopoles, and these now have the effect of turning a $\psi_\uparrow$ vortex into a $\psi_\downarrow$ vortex [80–82]. Again, as in (9.68), the y_m term in (9.83) is clearly a strongly relevant perturbation to $\mathcal{Z}_{2c,\mathrm{dual}}$ in (9.82). It ties the phases of $\psi_\uparrow$ and $\psi_\downarrow$ to each other, so that (9.83) is effectively the theory of a *single* complex scalar coupled to a non-compact U(1) gauge field B_μ. However, we have already considered such a theory in the *direct* representation in (9.57). We can now move from the dual representation in (9.83) back to the direct representation, by the mapping between (9.57) and (9.58). This leads to the conclusion, finally, that the theory (9.83) is dual to an ordinary XY model. In other words, the theory $\mathcal{Z}_2$ in (9.80) without its Berry phase term is an XY model. However, this is precisely the expected conclusion, and could have been easily reached without this elaborate series of duality mappings: just integrating over $A_{j\mu}$ for large e^2 yields an XY model in the angular field

$\theta_\uparrow - \theta_\downarrow$, which represents the orientation of the physical in-plane Néel order.

- Finally, let us look at the complete theory $\mathcal{Z}_2$. An explicit duality mapping can be carried out, and as in (9.70), the action (9.83) is replaced by [52, 71, 80, 81]

$$\mathcal{Z}_{2M,\mathrm{dual}} = \int \mathcal{D}\psi_a(r,\tau)\mathcal{D}B_\mu(r,\tau)\exp\Bigg(-\int d^2r d\tau\Bigg[|(\partial_\mu - iB_\mu)\psi_\uparrow|^2 + |(\partial_\mu + iB_\mu)\psi_\downarrow|^2 + \overline{s}|\psi_a|^2 + \frac{\overline{u}}{2}(|\psi_a|^2)^2 + \overline{v}|\psi_\uparrow|^2|\psi_\downarrow|^2 + \frac{1}{4\overline{e}^2}(\epsilon_{\mu\nu\lambda}\partial_\nu B_\lambda)^2 - y_{mq}\left((\psi_\uparrow\psi_\downarrow)^q + \left(\psi_\downarrow^*\psi_\uparrow^*\right)^q\right)\Bigg]\Bigg), \quad (9.84)$$

where the integer q was defined in (9.69). The subsequent reasoning is the precise analog of that for $N = 1$. For $S = 1/2$ and $q = 4$, the term proportional to y_{mq} representing q-fold monopole is irrelevant at the critical point (but not away from it in the paramagnetic phase). Consequently, the critical theory of (9.84) reduces to (9.82). So just as at $N = 1$, the *combined* influence of monopoles and Berry phases is dangerously irrelevant at the critical point, and for the critical theory we can take a naive continuum limit of $\mathcal{Z}_2$ neglecting both the Berry phases and the compactness of the gauge field.

We have now completed our discussion of the $N = 2$ easy plane model and established the existence of the same remarkable phenomenon found in Sect. 9.4.2.1 for $N = 1$, and claimed more generally [80, 81] at the beginning of Sect. 9.4.2 as the justification for the critical theory (9.55). As we saw in some detail in Sect. 9.4.1, monopoles, and attendant Berry phases, are absolutely crucial in understanding the onset of confinement and bond order in the paramagnetic phase. However, for $S = 1/2$, the Berry phases induce a destructive quantum interference between the monopoles at the quantum critical point, leading to a critical theory with 'deconfined' spinons and a non-compact U(1) gauge field which does not allow monopoles. These results are summarized in Table 2.

The results in Tables 1 and 2 can be generalized to arbitrary values of N, for models with the analog of an 'easy plane' anisotropy: as in (9.79), all the z_a have equal modulus and are expressed in terms of $a = 1 \ldots N$ angles θ_a. The dual models have N vortex fields ψ_a, and $N - 1$ non-compact U(1) gauge fields $B_{b\mu}$, $b = 1 \ldots (N-1)$. For $a = 1 \ldots (N-1)$, the field ψ_a has a charge $+1$ under the gauge field with $b = a$, and is neutral under all gauge fields with $b \neq a$. For $a = N$, the field ψ_N, has a charge -1 under *all* $N - 1$ gauge fields. (This gauge structure is similar to that found in 'moose' field theories [91].) The dual representation of the monopole operator is $\prod_{a=1}^{N}\psi_a$, and this appears as the coefficient of y_m (notice that this operator is neutral under all the gauge fields). The q^{th} power of this operator appears as the

Table 9.2. As in Table 1, but for the $N = 2$ easy plane case. The index a extends over the two values $\uparrow$, $\downarrow$. Again for $S = 1/2$, $q = 4$, the critical theory for the third row is the same as that for the first row. The dual model in the second row is effectively the theory of a single complex scalar coupled to a non-compact U(1) gauge field B_μ; by the inverse of the duality mapping in the first row of Table 1, this theory has a direct XY transition

$N = 2$, easy plane	
Direct lattice model	**Dual model**
$\mathcal{L}_{2,SC} = (1/(2e^2))\,(\epsilon_{\mu\nu\lambda}\Delta_\nu A_{j\lambda})^2 - (1/g)\cos(\Delta_\mu\theta_{ja} - A_{j\mu})$	$\mathcal{L}_{2SC,\mathrm{dual}} = \lvert(\partial_\mu - iB_\mu)\psi_\uparrow\rvert^2 + \lvert(\partial_\mu + iB_\mu)\psi_\downarrow\rvert^2 + \overline{s}\lvert\psi_a\rvert^2 + \frac{\overline{u}}{2}\left(\lvert\psi_a\rvert^2\right)^2 + \overline{v}\lvert\psi_\uparrow\rvert^2\lvert\psi_\downarrow\rvert^2 + \frac{1}{2\overline{e}^2}(\epsilon_{\mu\nu\lambda}\partial_\nu B_\lambda)^2$
$\mathcal{L}_{2M} = -(1/e^2)\cos(\epsilon_{\mu\nu\lambda}\Delta_\nu A_{j\lambda}) - (1/(2g))\cos(\Delta_\mu\theta_{ja} - A_{j\mu})$	$\mathcal{L}_{2M,\mathrm{dual}} = \lvert(\partial_\mu - iB_\mu)\psi_\uparrow\rvert^2 + \lvert(\partial_\mu + iB_\mu)\psi_\downarrow\rvert^2 + \overline{s}\lvert\psi_a\rvert^2 + \frac{\overline{u}}{2}\left(\lvert\psi_a\rvert^2\right)^2 + \overline{v}\lvert\psi_\uparrow\rvert^2\lvert\psi_\downarrow\rvert^2 + \frac{1}{2\overline{e}^2}(\epsilon_{\mu\nu\lambda}\partial_\nu B_\lambda)^2 - y_m\left(\psi_\uparrow\psi_\downarrow + \psi_\uparrow^*\psi_\downarrow^*\right)$
$\mathcal{L}_2 = -(1/e^2)\cos(\epsilon_{\mu\nu\lambda}\Delta_\nu A_{j\lambda}) - (1/g)\cos(\Delta_\mu\theta_{ja} - A_{j\mu}) - i2S\eta_j A_{j\tau}$	$\mathcal{L}_{2,\mathrm{dual}} = \lvert(\partial_\mu - iB_\mu)\psi_\uparrow\rvert^2 + \lvert(\partial_\mu + iB_\mu)\psi_\downarrow\rvert^2 + \overline{s}\lvert\psi_a\rvert^2 + \frac{\overline{u}}{2}\left(\lvert\psi_a\rvert^2\right)^2 + \overline{v}\lvert\psi_\uparrow\rvert^2\lvert\psi_\downarrow\rvert^2 + \frac{1}{2\overline{e}^2}(\epsilon_{\mu\nu\lambda}\partial_\nu B_\lambda)^2 - y_{mq}\left((\psi_\uparrow\psi_\downarrow)^q + \left(\psi_\uparrow^*\psi_\downarrow^*\right)^q\right)$

coefficient of y_{mq}. Note that the monopole operators involves a product of N fields, and for large enough N, *both* y_m and y_{mq} can be expected to be irrelevant perturbations at the quantum critical point.

Finally, these analyses of $\mathcal{Z}$ in (9.40) can be complemented by a study of its $N \to \infty$ limit, without any easy-plane anisotropy. This was carried out some time ago [51, 92], and it was found that monopoles were dangerously irrelevant at the quantum critical point, *both* with or without Berry phases

(as noted above for large N in the easy plane case). It is important to note that the situation at large N is subtly different from that for $N = 1, 2$: in the latter case, monopoles are dangerously irrelevant in the presence of $S = 1/2$ Berry phases, but relevant without Berry phases. The key understanding of this distinction emerged in the recent work of Senthil *et al.* [80, 81], which finally succeeded in placing the earlier large N results within the context of dual theories of topological defects in statistical mechanics.

9.5 Triangular Lattice Antiferromagnet

We continue our analysis of quantum antiferromagnets with an odd number of $S = 1/2$ spins per unit cell, but consider a class qualitatively different from those in Sect. 9.4. One of the defining properties of the models of Sect. 9.4 was that the magnetically ordered Néel state was defined by (9.2): the average magnetic moment on all sites were collinear, and only a single vector $\mathbf{n}$ was required to specify the orientation of the ground state. This section shall consider models in which the moments are *non-collinear*; the triangular lattice is the canonical example. However, similar results should also apply to other two-dimensional lattices with non-collinear ground states, such as the distorted triangular lattice found in Cs_2CuCl_4 [11].

We consider the model (9.28), but with the spins residing on the sites of the triangular lattice. This has a magnetically ordered state illustrated in Fig. 9.13; for this state (9.2) is replaced by

$$\langle \mathbf{S}_j \rangle = N_0 \left(\mathbf{n}_1 \cos(\boldsymbol{Q} \cdot \boldsymbol{r}) + \mathbf{n}_2 \sin(\boldsymbol{Q} \cdot \boldsymbol{r}) \right). \tag{9.85}$$

Here $\boldsymbol{Q} = 2\pi(1/3, 1/\sqrt{3})$ is the ordering wavevector, and $\mathbf{n}_{1,2}$ are two arbitrary orthogonal unit vectors in spin space

$$\mathbf{n}_1^2 = \mathbf{n}_2^2 = 1 \quad ; \quad \mathbf{n}_1 \cdot \mathbf{n}_2 = 0. \tag{9.86}$$

A distinct ground state, breaking spin rotation symmetry, is obtained for each choice of $\mathbf{n}_{1,2}$.

We now wish to allow the values of $\mathbf{n}_{1,2}$ to fluctuate quantum mechanically across spacetime, ultimately producing a paramagnetic state. As in Sect. 9.4, we should account for the Berry phases of each spin while setting up the effective action: an approach for doing this is presented in Sect. VI of [52]. However, the full structure of the critical theory is not understood in all cases, as we describe below.

One possible structure of the paramagnetic state is a confining, bond-ordered state, similar to that found in Sect. 9.4. However, there is no complete theory for a possible direct second-order transition from a non-collinear magnetically ordered state to such a paramagnet. Ignoring Berry phases, one could define the complex field $\Phi_\alpha = n_{1\alpha} + i n_{2\alpha}$, which, by (9.86), obeys

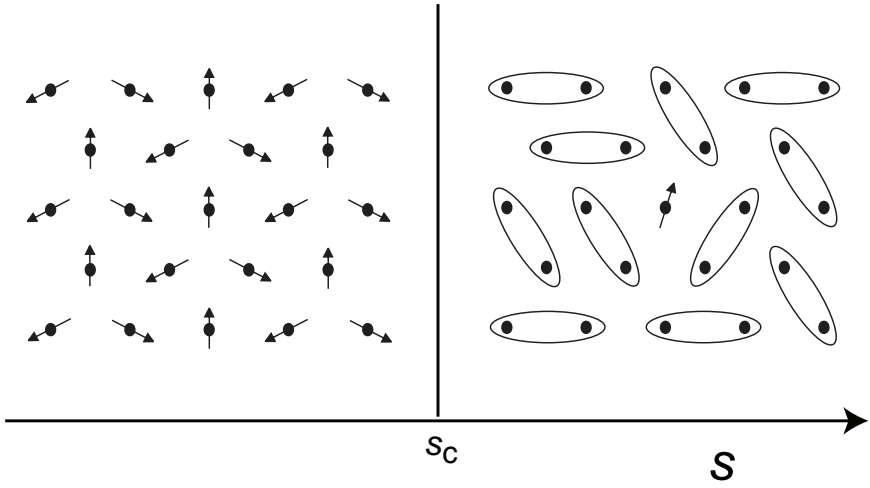

Fig. 9.13. Quantum phase transition described by $\mathcal{Z}_w$ in (9.90) as a function of s. The state on the left has non-collinear magnetic order described by (9.85). The state on the right is a 'resonating valence bond' (RVB) paramagnet with topological order and fractionalized $S = 1/2$ neutral spinon excitations (one spinon is shown above). Such a magnetically ordered state is observed in Cs_2CuCl_3 [11, 12], and there is evidence that the higher energy spectrum can be characterized in terms of excitations of the RVB state [24].

$\Phi_\alpha^2 = 0$, and then proceed to write down an effective action with the structure of (9.14). However, it is clear that such a theory describes a transition to a paramagnetic phase with a doublet of $S = 1$ triplet quasiparticles, and we can reasonably expect that such a phase has spontaneous bond order (in contrast to the explicit dimerization in the models of Sect. 9.2). Berry phases surely play an important role in inducing this bond order (as they did in Sect. 9.4.1), but there is no available theory for how this happens in the context of (9.14). Indeed, it is possible that there is no such direct transition between the non-collinear antiferromagnet and the bond-ordered paramagnet, and resolving this issue remains an important open question.

In contrast, it is possible to write down a simple theory for a direct transition between the non-collinear antiferromagnet and a paramagnetic phase not discussed so far: a resonating valence bond liquid [47,48,93] with *deconfined spinons and topological order*. This theory is obtained by observing that the constraints (9.86) can be solved by writing [94, 95]

$$\boldsymbol{n}_1 + i\boldsymbol{n}_2 \equiv \epsilon_{ab} w_b \boldsymbol{\sigma}_{ac} w_c, \tag{9.87}$$

where w_a is a 2 component complex spinor obeying $|w_\uparrow|^2 + |w_\downarrow|^2 = 1$. It is useful to compare (9.87) with (9.31), which parameterized a single vector also in terms of a complex spinor z_a. Whereas (9.31) was invariant under the

U(1) gauge transformation (9.32), notice that (9.87) is only invariant under the Z_2 gauge transformation

$$w_a(r,\tau) \to \varrho(r,\tau) w_a(r,\tau), \tag{9.88}$$

where $\varrho(r,\tau) = \pm 1$ is an arbitrary field which generates the gauge transformation. This Z_2 gauge transformation will play an important role in understanding the structure of the paramagnetic phase [21–23, 96, 97].

We can now study fluctuations of the non-collinear antiferromagnet by expressing the effective action in terms of the w_a. Apart from the familiar constraints of spin rotational invariance, and those imposed by (9.88), the effective action must also obey the consequences of translational invariance which follow from (9.85); the action must be invariant under

$$w_a \to w_a e^{-i\boldsymbol{Q}\cdot\boldsymbol{a}/2}, \tag{9.89}$$

where $\boldsymbol{a}$ is any triangular lattice vector. In the continuum limit, this leads to the following effective action

$$\mathcal{Z}_w = \int \mathcal{D}w_a(r,\tau) \exp\left(- \int d^2 r d\tau \left[|\partial_\mu w_a|^2 + s|w_a|^2 + \frac{u}{2}(|w_a|^2)^2 \right] \right); \tag{9.90}$$

notice there is a free integration over the w_a, and so we have softened the rigid length constraint. Comparing this with (9.55), we observe that the U(1) gauge field is now missing, and we simply have a Landau-Ginzburg theory for a 2 component complex scalar. The Z_2 gauge invariance (9.88) plays no role in this continuum critical theory for the destruction of non-collinear magnetic order, but as we discuss below, it will play an important role in the analysis of the paramagnetic phase. The theory (9.90) has a global O(4) invariance of rotations in the 4-dimensional space consisting of the real and imaginary parts of the 2 components of w_a: consequently the critical exponents of (9.90) are identical to those of the well known 4-component φ^4 field theory. Notice that there is no O(4) invariance in the microscopic theory, and this symmetry emerges only in the continuum limit [95,98]: the simplest allowed term which breaks this O(4) invariance is $|\epsilon_{ab} w_a \partial_\mu w_b|^2$, and this term is easily seen to be irrelevant at the critical point of the theory (9.90).

Let us now turn to a discussion of the nature of the paramagnetic phase obtained in the region of large positive s in (9.90). Here, the elementary excitations are free w_a quanta, and these are evidently $S = 1/2$ spinons. There is also a neutral, spinless topological excitation [21, 22, 99] whose importance was stressed in [97]: this is the 'vison' which is intimately linked with the Z_2 gauge symmetry (9.88). It is a point defect which carries Z_2 gauge flux. The vison has an energy gap in the paramagnetic phase, and indeed across the transition to the magnetically ordered state. This was actually implicit in our taking the continuum limit to obtain the action (9.90). We assumed

that all important spin configurations could be described by a smooth, single-valued field $w_a(r, \tau)$, and this prohibits vison defects around which the w_a are double-valued. It is also believed that the vison gap allows neglect of Berry phase effects across the transition described by (9.90): after duality, the Berry phases can be attached to monopoles and visons [97, 100], and these are suppressed in both phases of Fig. 9.13.

9.6 Conclusions

This article has described a variety of quantum phases of antiferromagnetic Mott insulators, and the transitions between them.

Let us first summarize the phases obtained in zero applied magnetic field, and transitions that can be tuned between them by varying the ratio of exchange constants in the Hamiltonian (experimentally, this can be achieved by applied pressure). The magnetically ordered states discussed were the collinear Néel state (shown in Figs. 9.4 and 9.12), and the non-collinear 'spiral' (shown in Fig. 9.13). We also found paramagnetic states which preserved spin rotation invariance and which had an energy gap to all excitations: these include the dimerized states (shown in Figs. 9.2 and 9.4), the related bond-ordered states which spontaneously break lattice symmetries (shown in Figs. 9.11 and 9.12), and the 'resonating valence bond' paramagnet with topological order and deconfined spinons (shown in Fig. 9.13). The continuous quantum phase transitions we found between these states were:
(a) the transition between the dimerized paramagnet and the collinear Néel state (both states shown in Fig. 9.4) was described by the theory $\mathcal{S}_\varphi$ in (9.12);
(b) the transition between the dimerized paramagnet and a non-collinear magnetically ordered state was described by $\mathcal{S}_\Phi$ in (9.14);
(c) the transition between the collinear Néel state and the paramagnet with *spontaneous* bond order (shown in Fig. 9.12) was described for $S = 1/2$ antiferromagnets by $\mathcal{Z}_c$ in (9.55);
(d) the transition between the state with non-collinear magnetic order and the RVB paramagnet (both states shown in Fig. 9.13) was described by $\mathcal{Z}_w$ in (9.90).

We also mention here other quantum transitions of Mott insulators, which involve distinct paramagnets on *both* sides of the critical point. These we did not discuss in the present paper, but such transitions have been discussed in the literature:
(e) the transition between a paramagnet with spontaneous bond order (Fig. 9.12) and a RVB paramagnet (Fig. 9.13) is described by a compact U(1) lattice gauge theory with charge 2 Higgs fields (closely related to $\mathcal{Z}_1$ in (9.56)), and is discussed in [81, 100, 101];
(f) transitions between paramagnets with different types of spontaneous bond order can be mapped onto transitions between different smooth phases of height models like (9.50), and are discussed in [102, 103].

Section 9.3 also considered quantum transitions that could be tuned by an applied magnetic field. We mainly considered the case of the coupled-dimer antiferromagnet, but very similar theories apply to the other states discussed above. The general theory has the structure of $\mathcal{S}_\Psi$ in (9.24), describing the Bose-Einstein condensation of the lowest non-zero spin quasiparticle excitation of the paramagnet. For the coupled dimer model this quasiparticle had $S = 1$, but an essentially identical theory would apply for cases with $S = 1/2$ spinon quasiparticles.

Acknowledgements

This research was supported by the National Science Foundation under grant DMR-0098226. I am grateful to Lorenz Bartosch, Gregoire Misguich, Flavio Nogueira, T. Senthil, and Asle Sudbø for valuable comments, and T. Senthil, Ashvin Vishwanath, Leon Balents, and Matthew Fisher for a fruitful recent collaboration [80, 81], upon which Sect. 9.4.2 is based, on the breakdown of Landau-Ginzburg-Wilson theory in Mott insulators.

References

1. S. Taniguchi, T. Nishikawa, Y. Yasui, Y. Kobayashi, M. Sato, T. Nishioka, M. Kotani, and S. Sano, J. Phys. Soc. Jpn. **64**, 2758 (1995).
2. G. Chaboussant, P. A. Crowell, L. P. Lévy, O. Piovesana, A. Madouri, and D. Mailly, Phys. Rev. B **55**, 3046 (1997).
3. P. R. Hammar, D. H. Reich, C. Broholm, and F. Trouw, Phys. Rev. B **57**, 7846 (1998).
4. M. B. Stone, Y. Chen, J. Rittner, H. Yardimci, D. H. Reich, C. Broholm, D. V. Ferraris, and T. Lectka, Phys. Rev. B **65**, 064423 (2002).
5. H. Kageyama, K. Yoshimura, R. Stern, N. V. Mushnikov, K. Onizuka, M. Kato, K. Kosuge, C. P. Slichter, T. Goto and Y. Ueda, Phys. Rev. Lett. **82**, 3168 (1999).
6. H. Kageyama, M. Nishi, N. Aso, K. Onizuka, T. Yosihama, K. Nukui, K. Kodama, K. Kakurai, and Y. Ueda, Phys. Rev. Lett. **84**, 5876 (2000).
7. H. Tanaka, A. Oosawa, T. Kato, H. Uekusa, Y. Ohashi, K. Kakurai, and A. Hoser, J. Phys. Soc. Jpn. **70**, 939 (2001).
8. A. Oosawa, M. Fujisawa, T. Osakabe, K. Kakurai, and H. Tanaka, J. Phys. Soc. Jpn **72**, 1026 (2003).
9. Ch. Rüegg, N. Cavadini, A. Furrer, H.-U. Güdel, K. Krämer, H. Mutka, A. Wildes, K. Habicht, and P. Vorderwisch, Nature (London) **423**, 62 (2003).
10. M. Matsumoto, B. Normand, T. M. Rice, and M. Sigrist, Phys. Rev. Lett. **89**, 077203 (2002) and cond-mat/0309440.
11. R. Coldea, D. A. Tennant, A. M. Tsvelik, and Z. Tylczynski, Phys. Rev. Lett. **86**, 1335 (2001).
12. R. Coldea, D. A. Tennant, and Z. Tylczynski, Phys. Rev. B **68**, 134424 (2003).

13. Insulators with an even number of electrons per unit cell can be adiabatically connected to band insulators, and so some readers may object to calling such materials 'Mott insulators'. However, the very different energy scales of the spin and charge excitations in the experimental systems are best understood in the framework of the Mott theory, and one regards the dimerization as a small, low energy, deformation. Following widely accepted practice, we will continue to label these materials Mott insulators.
14. S. Sachdev and R. N. Bhatt, Phys. Rev. B **41**, 9323 (1990).
15. A. V. Chubukov and Th. Jolicoeur Phys. Rev. B **44**, 12050 (1991).
16. V. N. Kotov, O. Sushkov, Z. Weihong, and J. Oitmaa, Phys. Rev. Lett. **80**, 5790 (1998).
17. G. Misguich and C. Lhuillier in *Frustrated spin systems*, H. T. Diep ed., World-Scientific, Singapore (2003), cond-mat/0310405.
18. The theorem of E. H. Lieb, T. Schultz, and D. J. Mattis, Ann. Phys. (N.Y.) **16**, 407 (1961) prohibits spin gap states in $d = 1$ systems with $S = 1/2$ per unit cell and no broken translational symmetry. For $d > 1$, the topological order to be discussed in Sect. 9.5 enables evasion of these constraints, as discussed *e.g.* in Appendix A of T. Senthil, M. Vojta, and S. Sachdev, cond-mat/0305193, and in G. Misguich, C. Lhuillier, M. Mambrini, and P. Sindzingre, Euro. Phys. Jour. B **26**, 167 (2002).
19. N. Read and S. Sachdev, Phys. Rev. Lett. **62**, 1694 (1989).
20. N. Read and S. Sachdev, Phys. Rev. B **42**, 4568 (1990).
21. N. Read and S. Sachdev, Phys. Rev. Lett. **66**, 1773 (1991).
22. S. Sachdev and N. Read, Int. J. Mod. Phys. B **5**, 219 (1991); available online at http://onsager.physics.yale.edu/p34.pdf.
23. X. G. Wen, Phys. Rev. B **44**, 2664 (1991).
24. C.-H. Chung, K. Voelker, and Y.-B. Kim, Phys. Rev. B **68**, 094412 (2003).
25. M. P. Gelfand, R. R. P. Singh, and D. A. Huse, Phys. Rev. B **40**, 10801 (1989).
26. J. Callaway, *Quantum Theory of the Solid State*, Academic Press, New York (1974).
27. K. P. Schmidt and G. S. Uhrig, Phys. Rev. Lett. **90**, 227204 (2003).
28. M. Matsumoto, C. Yasuda, S. Todo, and H. Takayama, Phys. Rev. B **65**, 014407 (2002).
29. T. Sommer, M. Vojta, and K. W. Becker, Eur. Phys. J. B **23**, 329 (2001).
30. D. Carpentier and L. Balents, Phys. Rev. B **65**, 024427 (2002).
31. M. Itakura, J. Phys. Soc. Jpn. **72** 74 (2003).
32. B. Normand and T. M. Rice Phys. Rev. B **54**, 7180 (1996); Phys. Rev. B **56**, 8760 (1997).
33. S. Chakravarty, B. I. Halperin, and D. R. Nelson, Phys. Rev. B **39**, 2344 (1989).
34. K. Chen, A. M. Ferrenberg, and D. P. Landau, Phys. Rev. B **48**, 3249 (1993).
35. S.-k Ma, *Modern Theory of Critical Phenomena*, W. A. Benjamin, Reading, Mass. (1976).
36. S. Sachdev and J. Ye, Phys. Rev. Lett. **69**, 2411 (1992).
37. A. V. Chubukov, S. Sachdev, and J. Ye, Phys. Rev. B **49**, 11919 (1994).
38. K. Damle and S. Sachdev, Phys. Rev. B **56**, 8714 (1997).
39. E. Demler, S. Sachdev, and Y. Zhang, Phys. Rev. Lett. **87**, 067202 (2001); Y. Zhang, E. Demler, and S. Sachdev, Phys. Rev. B **66**, 094501 (2002).
40. I. Affleck, Phys. Rev. B **41**, 6697 (1990).
41. S. Sachdev, T. Senthil, and R. Shankar, Phys. Rev. B **50**, 258 (1994).

42. M. P. A. Fisher, P. B. Weichman, G. Grinstein, and D. S. Fisher, Phys. Rev. B **40**, 546 (1989).
43. Y. Shindo and H. Tanaka, cond-mat/0310691.
44. M. Oshikawa, M. Yamanaka, and I. Affleck, Phys. Rev. Lett. **78**, 1984 (1997).
45. H. Kageyama, K. Yoshimura, R. Stern, N. V. Mushnikov, K. Onizuka, M. Kato, K. Kosuge, C. P. Slichter, T. Goto, and Y. Ueda, Phys. Rev. Lett. **82**, 3168 (1999); K. Onizuka, H. Kageyama, Y. Narumi, K. Kindo, Y. Ueda, and T. Goto, J. Phys. Soc. Jpn. **69**, 1016 (2000); S. Miyahara, F. Becca, and F. Mila, Phys. Rev. B **68**, 024401 (2003).
46. W. Shiramura, K. Takatsu, B. Kurniawan, H. Tanaka, H. Uekusa, Y. Ohashi, K. Takizawa, H. Mitamura, and T. Goto, J. Phys. Soc. Jpn. **67**, 1548 (1998).
47. P. Fazekas and P. W. Anderson, Philos. Mag. **30**, 23 (1974).
48. S. A. Kivelson, D. S. Rokhsar, and J. P. Sethna, Phys. Rev. B **35**, 8865 (1987).
49. S. Sachdev, *Quantum Phase Transitions* (Cambridge University Press, Cambridge, England, 1999).
50. B. Berg and M. Lüscher, Nucl. Phys. B **190**, 412 (1981).
51. S. Sachdev and R. Jalabert, Mod. Phys. Lett. B **4**, 1043 (1990); available online at http://onsager.physics.yale.edu/p32.pdf.
52. S. Sachdev and K. Park, Annals of Physics, N.Y. **298**, 58 (2002).
53. A. D'Adda, P. Di Vecchia, and M. Lüscher, Nucl. Phys. B **146**, 63 (1978).
54. E. Witten, Nucl. Phys. B **149**, 285 (1979).
55. S. Sachdev, *Proceedings of the International Conference on Theoretical Physics*, Paris, Annales Henri Poincare **4**, 559 (2003).
56. J. Villain, J. Phys. (Paris) **36**, 581 (1975).
57. J. V. José, L. P. Kadanoff, S. Kirkpatrick, and D. R. Nelson, Phys. Rev. B **16**, 1217 (1977).
58. E. Fradkin and S. A. Kivelson, Mod. Phys. Lett. B **4**, 225 (1990).
59. S. T. Chui and J. D. Weeks, Phys. Rev. B **14**, 4978 (1976); D. S. Fisher and J. D. Weeks, Phys. Rev. Lett. **50**, 1077 (1983); E. Fradkin Phys. Rev. B **28**, 5338 (1983).
60. A. M. Polyakov, *Gauge Fields and Strings*, Harwood Academic, New York (1987).
61. I. Affleck, T. Kennedy, E. H. Lieb, and H. Tasaki, Phys. Rev. Lett. **59**, 799 (1987).
62. W. Zheng and S. Sachdev, Phys. Rev. B **40**, 2704 (1989).
63. D. Rokhsar and S. A. Kivelson, Phys. Rev. Lett. **61**, 2376 (1988).
64. J.-S. Bernier, C.-H. Chung, Y. B. Kim, and S. Sachdev, cond-mat/0310504.
65. K. Rommelse and M. den Nijs, Phys. Rev. Lett. **59**, 2578 (1987).
66. J.-B. Fouet, P. Sindzingre, and C. Lhuillier, Eur. Phys. J. B **20**, 241 (2001).
67. W. Brenig and A. Honecker, Phys. Rev. B **64**, 140407 (2002).
68. J.-B. Fouet, M. Mambrini, P. Sindzingre, and C. Lhuillier, Phys. Rev. B **67**, 054411 (2003).
69. C.-H. Chung, J. B Marston, and S. Sachdev, Phys. Rev. B **64**, 134407 (2001).
70. A. W. Sandvik, S. Daul, R. R. P. Singh, and D. J. Scalapino, Phys. Rev. Lett., **89**, 247201 (2002).
71. C. Lannert, M. P. A. Fisher, and T. Senthil, Phys. Rev. B **63**, 134510 (2001).
72. K. Park and S. Sachdev, Phys. Rev. B **65**, 220405 (2002).
73. K. Harada, N. Kawashima, and M. Troyer, Phys. Rev. Lett. **90**, 117203 (2003).

74. V. N. Kotov, J. Oitmaa, O. P. Sushkov, and Z. Weihong, Phys. Rev. B **60**, 14613 (1999); R. R. P. Singh, Z. Weihong, C. J. Hamer, and J. Oitmaa, Phys. Rev. B **60**, 7278 (1999); V. N. Kotov and O. P. Sushkov, Phys. Rev. B **61**, 11820 (2000); O. P. Sushkov, J. Oitmaa, and Z. Weihong, Phys. Rev. B **66**, 054401 (2002).
75. M. S. L. du Croo de Jongh, J. M. J. van Leeuwen, and W. van Saarloos, Phys. Rev. B **62**, 14844 (2000).
76. E. Dagotto and A. Moreo, Phys. Rev. Lett. **63**, 2148 (1989); R. R. P. Singh and R. Narayanan, Phys. Rev. Lett. **65**, 1072 (1990); H. J. Schulz and T. A. L. Ziman, Europhys. Lett. **18**, 355 (1992); H. J. Schulz, T. A. L. Ziman, and D. Poilblanc, J. Phys. I (France) **6**, 675 (1996).
77. L. Capriotti, F. Becca, A. Parola, and S. Sorella, Phys. Rev. Lett. **87**, 097201 (2001).
78. O. P. Sushkov, Phys. Rev. B **63**, 174429 (2001).
79. R. Eder and Y. Ohta, cond-mat/0304554 and cond-mat/0308184.
80. T. Senthil, A. Vishwanath, L. Balents, S. Sachdev, and M. P. A. Fisher, to appear in Science, cond-mat/0311326.
81. T. Senthil, L. Balents, S. Sachdev, A. Vishwanath, M. P. A. Fisher, cond-mat/0312617.
82. O. Motrunich and A. Vishwanath, cond-mat/0311222.
83. M. Vojta and S. Sachdev, Phys. Rev. Lett. **83**, 3916 (1999); M. Vojta, Y. Zhang, and S. Sachdev, Phys. Rev. B **62**, 6721 (2000).
84. C. Dasgupta and B. I. Halperin, Phys. Rev. Lett. **47**, 1556 (1981).
85. See *e.g.* D. J. Amit, *Field theory, the renormalization group, and critical phenomena*, World Scientific, Singapore (1984).
86. H. Kleinert, F. S. Nogueira, and A. Sudbø, Phys. Rev. Lett. **88**, 232001 (2002); Nucl. Phys. B **666**, 316 (2003).
87. N. Nagaosa and P. A. Lee, Phys. Rev. B **61**, 9166 (2000).
88. For completeness, we mention that the mapping to the dual XY model in a field has been questioned in I. Ichinose, T. Matsui, and M. Onoda, Phys. Rev. B **64**, 104516 (2001), and [86]. The duality mappings in [80,81] do not support these claims.
89. F. D. M. Haldane, Phys. Rev. Lett. **61**, 1029 (1988).
90. J. M. Carmona, A. Pelissetto, and E. Vicari, Phys. Rev. B **61**, 15136 (2000).
91. N. Arkani-Hamed, A. G. Cohen, and H. Georgi, Phys. Rev. Lett. **86**, 4757 (2001); C. T. Hill, S. Pokorski, and J. Wang, Phys. Rev. D **64** 105005 (2001).
92. G. Murthy and S. Sachdev, Nucl. Phys. B **344**, 557 (1990).
93. R. Moessner and S. L. Sondhi, Phys. Rev. Lett. **86**, 1881 (2001).
94. A. Angelucci, Phys. Rev. B **45**, 5387 (1992).
95. A. V. Chubukov, T. Senthil and S. Sachdev, Phys. Rev. Lett. **72**, 2089 (1994).
96. S. Sachdev, Phys. Rev. B **45**, 12377 (1992).
97. T. Senthil and M. P. A. Fisher, Phys. Rev. B **62**, 7850 (2000).
98. P. Azaria, B. Delamott, and T. Jolicoeur, Phys. Rev. Lett. **64**, 3175 (1990); P. Azaria, B. Delamott and D. Mouhanna, Phys. Rev. Lett. **68**, 1762 (1992).
99. N. Read and B. Chakraborty, Phys. Rev. B **40**, 7133 (1989).
100. R. Jalabert and S. Sachdev, Phys. Rev. B **44**, 686 (1991).
101. S. Sachdev and M. Vojta, J. Phys. Soc. Jpn. **69**, Suppl. B, 1 (2000).
102. A. Vishwanath, L. Balents, and T. Senthil, cond-mat/0311085.
103. E. Fradkin, D. A. Huse, R. Moessner, V. Oganesyan, and S. L. Sondhi, cond-mat/0311353; E. Ardonne, P. Fendley, and E. Fradkin, cond-mat/0311466.